LYSOSOMAL STORAGE DISEASES

Heat shock protein–based therapy as a potential candidate for treating the sphingolipidoses

Thomas Kirkegaard,[1]*† James Gray,[2]* David A. Priestman,[2] Kerri-Lee Wallom,[2] Jennifer Atkins,[2] Ole Dines Olsen,[1,3] Alexander Klein,[4] Svetlana Drndarski,[5] Nikolaj H. T. Petersen,[1] Linda Ingemann,[1] David A. Smith,[2] Lauren Morris,[2] Claus Bornæs,[1] Signe Humle Jørgensen,[1] Ian Williams,[2] Anders Hinsby,[1] Christoph Arenz,[4] David Begley,[5] Marja Jäättelä,[3]* Frances M. Platt[2]*

Lysosomal storage diseases (LSDs) often manifest with severe systemic and central nervous system (CNS) symptoms. The existing treatment options are limited and have no or only modest efficacy against neurological manifestations of disease. We demonstrate that recombinant human heat shock protein 70 (HSP70) improves the binding of several sphingolipid-degrading enzymes to their essential cofactor bis(monoacyl)glycerophosphate in vitro. HSP70 treatment reversed lysosomal pathology in primary fibroblasts from 14 patients with eight different LSDs. HSP70 penetrated effectively into murine tissues including the CNS and inhibited glycosphingolipid accumulation in murine models of Fabry disease (*Gla*$^{-/-}$), Sandhoff disease (*Hexb*$^{-/-}$), and Niemann-Pick disease type C (*Npc1*$^{-/-}$) and attenuated a wide spectrum of disease-associated neurological symptoms in *Hexb*$^{-/-}$ and *Npc1*$^{-/-}$ mice. Oral administration of arimoclomol, a small-molecule coinducer of HSPs that is currently in clinical trials for Niemann-Pick disease type C (NPC), recapitulated the effects of recombinant human HSP70, suggesting that heat shock protein–based therapies merit clinical evaluation for treating LSDs.

INTRODUCTION

Lysosomal storage diseases (LSDs) are caused by mutations in lysosomal proteins, their activator proteins, or proteins required for their intracellular transport (*1*). These diseases are characterized by accumulation of undegraded macromolecules in lysosomes and eventually in other cellular compartments. Their clinical manifestations depend on the spatiotemporal relationship of the affected protein, its substrate, and its role during normal development and physiology. For example, defects in glycosphingolipid (GSL) turnover often result in severe neurological manifestations because of the essential role of GSLs in CNS development (*2*).

Because of the ability of molecular chaperones of the heat shock protein 70 (HSP70) family to protect pathologically challenged cells, HSP70-based therapies are emerging as attractive treatment options for many degenerative diseases (*3*–*8*). Notably, the cytoprotective effect of the major stress-inducible member of the family, HSP70 (HSPA1A), involves direct interactions with lysosomes (*6*, *9*–*11*). HSP70 binds with high affinity to lysosomal bis(monoacylglycero)phosphate (BMP), a phospholipid cofactor of lysosomal sphingolipid catabolism (*2*, *6*, *12*–*18*). This interaction stabilizes the association of acid sphingomyelinase (ASM) with BMP containing intralysosomal membranes, thereby tethering ASM to its substrate and protecting it from degradation. The subsequent increase in ASM activity and improved catabolism of sphingomyelin to ceramide counteracts lysosomal aggregation and membrane permeabilization, which are hallmarks of LSDs and stress-induced cell death (*9*, *19*–*26*).

After the discoveries of the role of HSP70 in lysosomal pathologies (*6*, *9*), a number of recent publications have reported improved enzyme activities and lysosomal pathologies through the induction of HSPs in various LSDs (*6*, *9*, *27*–*32*). As a consequence, the induction of HSPs is emerging as an attractive therapeutic target in LSDs, for example, in Niemann-Pick disease type C (NPC), where HSP70 has recently been demonstrated to be critical for the proper folding and activity of the NPC1 protein (*29*, *33*). It is therefore likely that HSP70 may have dual benefits in this disease by not only chaperoning mutant proteins but also protecting against permeabilization of lysosomes.

A critical aspect of therapeutically targeting HSP regulation is to accomplish this in a safe and well-tolerated way, particularly for chronic diseases such as the LSDs. In contrast to other reported inducers of HSPs that work by inducing cell stress, the clinically enabled small-molecule HSP coinducer arimoclomol has been tested in a number of clinical trials (*34*, *35*). Arimoclomol belongs to a group of HSP-modulating drugs that act as coinducers of HSPs, particularly HSP70, whose mechanism of action involves stabilizing the interaction of heat shock factor 1 (HSF1) with heat shock elements (HSEs), the transcriptional elements controlling HSP production (*3*, *5*, *7*, *36*–*38*).

RESULTS

rHSP70 enhances BMP binding of sphingolipases and reverses lysosomal pathology in cells from LSD patients

We previously reported the ability of recombinant HSP70 (rHSP70) to enhance the activity of mutant ASM and to reverse the lysosomal pathology in fibroblasts from Niemann-Pick disease A and B (NPDA/B) through its interaction with BMP (*6*). We hypothesized that the same mechanism could also increase the binding of other sphingolipid-degrading enzymes to BMP and alleviate the lysosomal storage pathologies of other LSDs. We therefore analyzed the effects of rHSP70's interaction with BMP for other known BMP-interacting lysosomal enzymes and the effects on lysosomal pathology (Fig. 1, A to C). rHSP70 facilitated the BMP binding of Alexa Fluor 488 (AF488)–labeled

[1]Orphazyme ApS, Copenhagen, Denmark. [2]Department of Pharmacology, University of Oxford, Oxford, U.K. [3]Cell Death and Metabolism Unit, Center for Autophagy, Recycling, and Metabolism, Danish Cancer Society Research Center, Copenhagen, Denmark. [4]Institut für Chemie der Humboldt-Universität zu Berlin, Berlin, Germany. [5]Institute of Pharmaceutical Science, King's College London, London, U.K.
*These authors contributed equally to this work.
†Corresponding author. Email: tkj@orphazyme.com

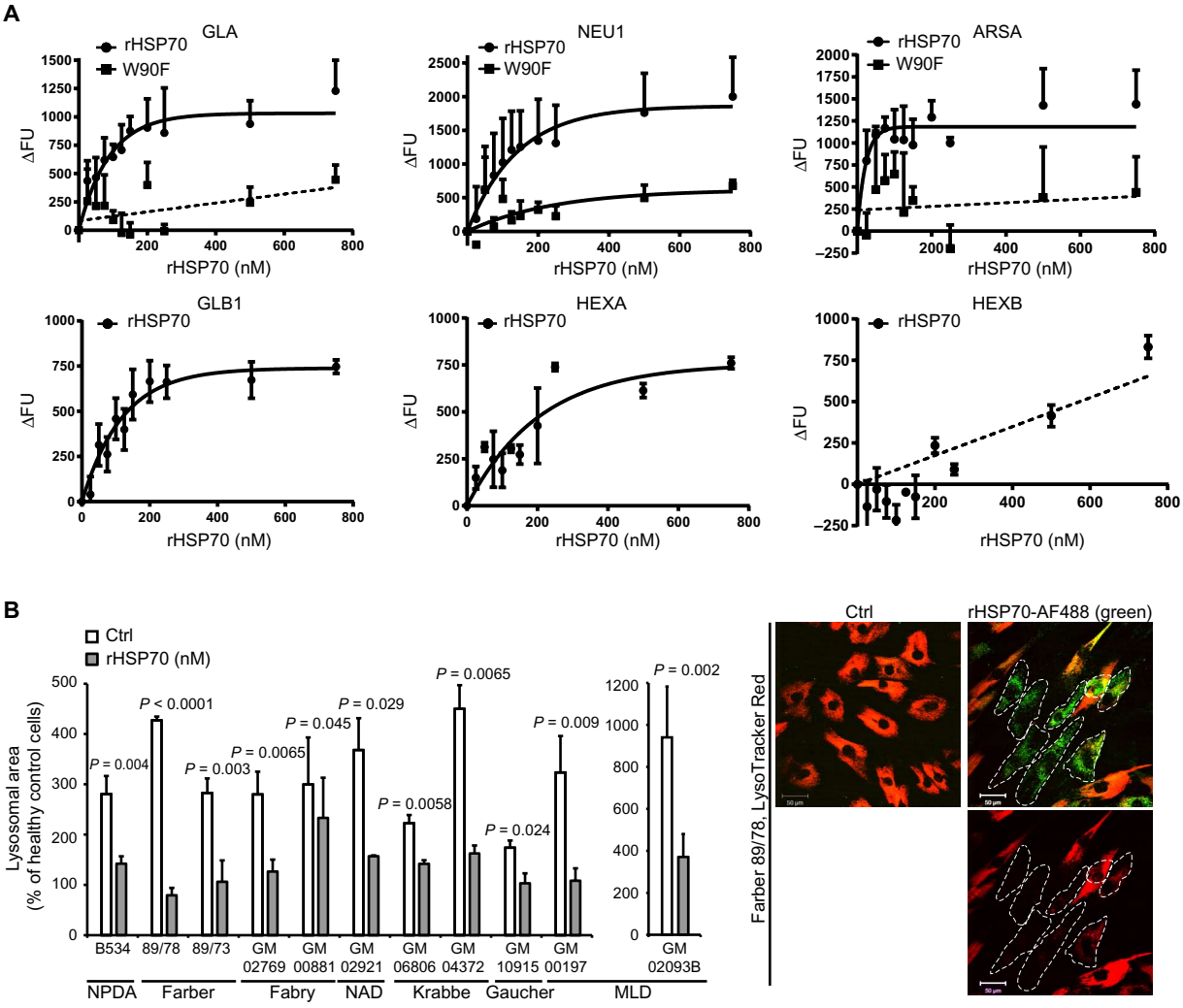

Fig. 1. Effects of rHSP70 treatment in vitro. (**A**) Analysis of rHSP70's effect on the lipid cofactor BMP-binding interactions of sphingolipid catabolic enzymes (GLA, NEU1, ARSA, GLB1, HEXA, and HEXB). Data points and association curves (non-linear regression, assuming one-phase association) are depicted on all graphs for rHSP70 except for HEXB (no curve fit). For GLA, NEU1, and ARSA, the effect of the Trp90Phe point mutation in HSP70 (W90F) lacking the capacity to interact with BMP was also analyzed. Only for NEU1 could a one-phase association curve be fitted. For ARSA and GLA, the signal was too weak to establish any meaningful regression (linear regression shown as a guide). FU, fluorescence units. (**B**) Quantification of lysosomal area in confocal cross sections of primary fibroblasts from patients with different LSDs, either sham-treated (Vehicle) or treated for 24 hours with 300 nM rHSP70. The representative microscopic images on the right show the effect of 24-hour rHSP70 (green) treatment on the volume of the lysosomal compartment (red) in fibroblasts from a patient with Farber disease. White dotted lines indicate the positions of cells with endocytosed rHSP70. Scale bars, 50 μm. (**C**) Quantification of lysosomal area of confocal cross sections of primary patient fibroblasts from patients with NPC, either sham-treated or treated for 24 hours with 300 nM rHSP70. GM numbers (GM17918, etc.) are cell line identifiers at the Coriell Cell Repository. (**D**) Quantification of lysosomal area of confocal cross sections of primary patient fibroblasts from two NPDA patients treated with 300 nM of the indicated recombinant proteins for 24 hours. (A) The individual values represent the mean of three independent experiments ($P \leq 0.05$). (B to D) All values represent means ± SD for a minimum of three independent experiments. A minimum of 100 cells were analyzed for each independent experiment ($P \leq 0.05$). Two-sample comparisons were performed by using Student's *t* test, and multiple comparisons were analyzed by one-way analysis of variance (ANOVA) followed by Dunnett's multiple comparison test.

recombinant α-galactosidase A (GLA), α-galactosidase B1 (GLB1), neuraminidase 1 (NEU1), arylsulfatase A (ARSA), and β-hexosaminidase A (HEXA) in a dose-dependent manner with maximal effect of about 200 nM. In contrast, β-hexosaminidase B (HEXB) binding to BMP was enhanced only marginally at higher rHSP70 concentrations (Fig. 1A). Similar concentrations of the rHSP70-W90F mutant, which is incapable of binding to BMP (*6*), showed limited or no effect on the BMP binding of other sphingolipid-degrading enzymes (Fig. 1A). Given the ability of rHSP70 to promote the BMP binding of most of the tested sphingolipid-degrading enzymes, we investigated whether it could reverse the LSD-associated enlargement of the lysosomal compartment in primary fibroblasts from patients with six different sphingolipidoses, including Farber disease, Fabry disease, Gaucher disease, Krabbe disease, neuraminidase deficiency, and metachromatic leukodystrophy (MLD). Similar to fibroblasts from NPDA/B patients, all patient cells had a pathologically enlarged lysosomal compartment, which was effectively corrected by a 24-hour treatment with rHSP70 (Fig. 1B). Furthermore, rHSP70 improved endolysosomal dynamics in fibroblasts from patients with NPD (movies S1 and S2). As with the primary sphingolipidoses, rHSP70 reversed the lysosomal pathology in primary fibroblasts from patients suffering from NPC1 (Fig. 1C), which is caused by mutations in an endolysosomal transporter. Such mutations result in lysosomal lipid accumulation and reduced ASM activity, both of which have been linked to disease progression (*39*–*42*). The effect on lysosomal pathology appeared specific to the stress-inducible HSP70, as homologous cytosolic family members (Hsc70 and HSP70-2) (*43*) as well as other HSPs with well-documented effects on cellular metabolism and survival (HSP27 and HSP90) (*4*, *44*) failed to reverse lysosomal accumulation in NPDA fibroblasts (Fig. 1D).

rHSP70 distributes to peripheral tissues and the brains of mice after intravenous or intraperitoneal administration

To assess the feasibility of rHSP70 as a potential biological therapy for LSDs, we investigated its pharmacological properties including the longevity and reversibility of its effects. We also performed pharmacokinetic (PK) and distribution studies (Fig. 2 and fig. S1). For the PK and distribution studies, we used complementary autoradiographic (^{125}I-labeled rHSP70) and immunological methods [enzyme-linked immunosorbent assay (ELISA)] to analyze the PK and organ distribution of rHSP70 after both intravenous and intraperitoneal injections. Recombinant human HSP70 (rhHSP70) was effectively taken up by both patient fibroblasts and lymphocytes (fig. S1). The effect of a single administration of rHSP70 on the aggregation of lysosomes in primary fibroblasts from NPDA patients disappeared gradually over the course of a week (Fig. 2A). Repeated weekly administration resulted in a sustained reduction of lysosomal storage burden (Fig. 2A). The analysis of the organ distribution of rHSP70 after single intravenous or intraperitoneal administration to mice showed dose-dependent profiles in all studied peripheral organs but interestingly also mouse brain as analyzed by both autoradiography and ELISA (Fig. 2, B and C, and fig. S8). As the potential to target the CNS is of significant therapeutic importance, we used an additional four complementary methods to confirm and characterize the distribution of rHSP70 in the brain: (i) microdialysis probe insertion into the dorsal striatum of freely moving rats (*45*), (ii) capillary spin-down (*46*), (iii) immunohistochemistry, and (iv) multiple-time regression analysis that determines the blood-to-brain influx constant (*47*). All four methods showed that rHSP70 crosses the blood-brain barrier to a significant extent and most importantly enters neurons (Fig. 2, F to I). The blood-to-brain transfer ratios indicated that rHSP70 entered the brain via receptor-mediated transport (Fig. 2I) with different brain regions showing differential penetration rates of rHSP70, the midbrain having the highest uptake rate (Fig. 2I and Table 1).

Effective CNS uptake appeared to be mediated by receptor-mediated transport by the low-density lipoprotein receptor–related protein 1 receptor (LRP1/A2MR/APOER/CD91) (*48*–*53*). We therefore tested the contribution of LRP1 to rHSP70's lysosomal effects. We treated NPDA patient fibroblasts with α_2-macroglobulin (A2M), the native ligand of LRP1. A2M efficiently competed with rHSP70 for uptake (Fig. 2D) but did not affect lysosomal storage itself (Fig. 2E). These data demonstrate that LRP1 was responsible for the observed rHSP70 endocytosis in patient fibroblasts and that receptor engagement and activation by itself was not sufficient to elicit the reduction in lysosomal storage observed upon administration of rHSP70 (*6*). Together, these data demonstrate that rHSP70 has a favorable distribution profile as it effectively reached all tissues including the heart and CNS, tissues that have been difficult to target and therefore treat with existing enzyme replacement therapies (*54*).

rHSP70 attenuates GSL accumulation in a murine model of Fabry disease

Prompted by the in vitro activities and pharmacological properties of rHSP70, we proceeded to test its efficacy in three murine models of sphingolipid storage diseases, that is, *Gla*$^{-/-}$, *HexB*$^{-/-}$, and *Npc1*$^{-/-}$ mice serving as models for Fabry disease, Sandhoff disease, and early-onset NPC diseases, respectively (*55*–*58*). *Gla*$^{-/-}$ mice have previously been used as a biochemical model of Fabry disease to demonstrate preclinical efficacy of enzyme replacement therapies through reduction of biochemical storage of the GLA substrate globotriaosylceramide (Gb3) in the kidneys (*59*). Gb3 has subsequently been shown to be a relevant biomarker for Fabry disease (*60*). This mouse model has also been shown to be responsive to substrate reduction therapies, consistent with a GLA-independent salvage pathway for Gb3 degradation (*61*). To evaluate the efficacy of rHSP70 in this model, we treated *Gla*$^{-/-}$ mice with three weekly injections of rHSP70 (5 mg/kg) starting at the age of 3 weeks. At 17 weeks of age, the mice were sacrificed and kidneys, hearts, and dorsal root ganglia were harvested to assess the accumulation of the major GLA substrate, Gb3. Both kidneys and hearts of the rHSP70-treated mice showed a significant reduction of Gb3 ($P \leq 0.05$; Fig. 3, A and B). We also determined storage amounts of Gb3 in the cell bodies of the peripheral nervous system by analyzing the dorsal root ganglia, because peripheral pain is one of the clinical features of Fabry disease. The dorsal root ganglia of the *Gla*$^{-/-}$ mice showed progressive storage of not only Gb3 but also other Gb3 derivatives, the so-called isogloboseries (Fig. 3, C and D), consistent with previous reports (*62*). Male mice had a significantly higher accumulation of Gb3 and its derivatives in dorsal root ganglia than females, whereas the gender differences in heart and kidney were negligible (Fig. 3D). The administration of rHSP70 significantly reduced the accumulation of all stored GSL species (globoside and isogloboside series) in the dorsal root ganglia of male and female mice ($P \leq 0.05$; Fig. 3, E and F). These data show that rHSP70 can reduce the accumulation of GSLs in a translationally relevant model of Fabry disease.

rHSP70 attenuates GSL accumulation and disease progression in a murine model of Sandhoff disease

Next, we tested the efficacy of a similar rHSP70 treatment protocol in the *HexB*$^{-/-}$ mice, which, despite some metabolic and pathological

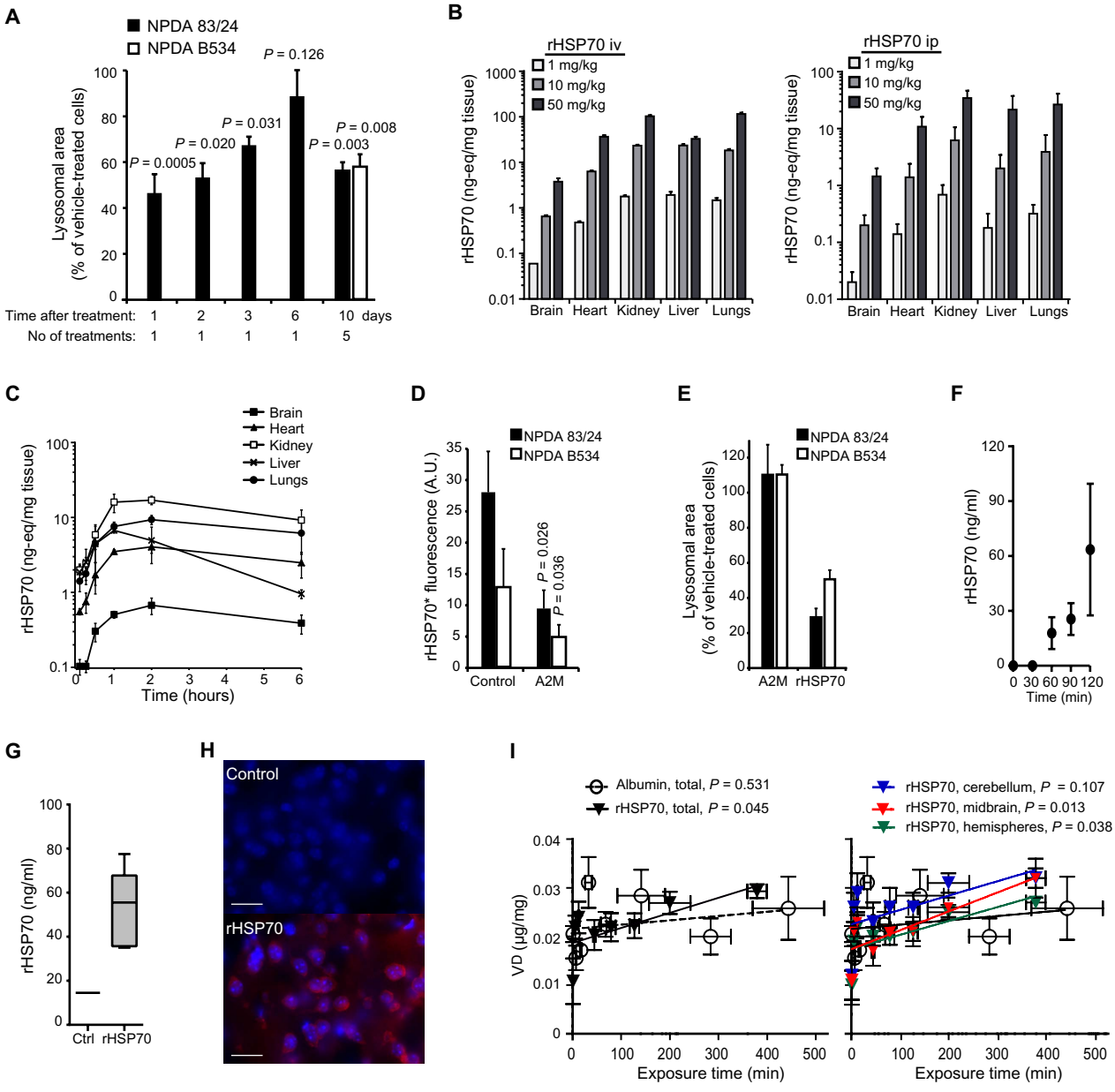

Fig. 2. PK and distribution of rHSP70. (**A**) Quantification of lysosomal area in confocal cross sections from primary fibroblasts from an NPDA patient (83/24) treated with 300 nM rHSP70 for 24 hours followed by a chase period of 1, 2, 3, or 6 days. Quantification of lysosomal area of confocal cross sections from primary fibroblasts from two NPDA patients at the end of a series of repeated exposures to 300 nM rHSP70 for 24 hours once weekly for 5 weeks total ($P \leq 0.01$). Two-sample comparisons were performed by using Student's *t* test. (**B**) Dose dependence of tissue distribution after administration of ^{125}I-rHSP70 (1, 10, or 50 mg/kg) for 15 min [intravenously (iv)] or 60 min [intraperitoneally (ip)] ($n = 3$ per dose, values represent means ± SD). (**C**) Time dependence of tissue distribution after intraperitoneal administration of ^{125}I-rHSP70 (10 mg/kg) ($n = 3$ per time point, values represent means ± SD). (**D**) Analysis of the effect of the LRP1 ligand A2M on the receptor-mediated uptake of rHSP70 ($P \leq 0.05$). Two-sample comparisons were performed by using Student's *t* test. (**E**) Quantification of lysosomal area of confocal cross sections from primary fibroblasts from two NPDA patients, treated with either 300 nM A2M or rHSP70 for 24 hours. A.U., arbitrary units. (**F**) Effect of administered rHSP70 (10 mg/kg iv) on free HSP70 levels in the striatum of adult male Wistar rat brains. rHSP70 was infused from $t = 0$ ($n = 4$, values represent means ± SD). (**G**) Amount of rHSP70 in adult male Wistar rat brain after administration of rHSP70 (10 mg/kg iv) for 120 min followed by saline perfusion and capillary spin-down ($n = 6$ for rHSP70-treated and $n = 1$ for saline infusion control). Box and whisker plot depicts minimum to maximum. (**H**) Immunohistochemical analysis of cortical sections from *Npc1*$^{-/-}$ mice administered phosphate-buffered saline (PBS) (Control) or rHSP70 (3 mg/kg ip, three times per week) for 4 weeks. Scale bars, 25 µm. (**I**) Patlak plots (multiple time regression analysis) of the volume of distribution for injected ^{3}H-albumin or ^{3}H-rHSP70 (20 mg/kg iv) against the plasma area under the curve in either whole brain (left graph), cerebellum, midbrain, or left and right hemispheres (right graph) ($n = 4$ to 7 mice per time point).

differences compared to patients with Sandhoff disease, present with similar ganglioside accumulation in the CNS and ataxia (*57*, *58*). This mouse model was previously used to study the effects of substrate reduction therapies and presents with a relatively uniform disease progression with little biological variability (*63*). Administration of rHSP70 significantly reduced the accumulation of GSLs, including the major storage lipid gangliosides A2 and M2 (GA2 and GM2), in the mouse brain and had a modest effect on the accumulation of the major storage metabolite GA2 in the liver ($P \leq 0.05$; Fig. 4, A and B). The observed biochemical effects were accompanied by a significant reduction in ataxia as measured by quantitative gait analysis ($P \leq 0.05$; Fig. 4B). The treatment failed, however, to convey any significant improvement in a bar crossing test, suggesting that rHSP70 improves motor coordination rather than muscle strength. The final set of experiments with continued HSP70 treatment revealed a modest but significant impact on survival of 15% ($P = 0.0018$; Fig. 4C). All treated animals lived beyond the age of the longest-living control animal but then relatively uniformly succumbed within a short time span, suggesting that the positive benefits of rHSP70 were somehow abrogated. We therefore measured the antidrug antibody titers in the serum of the rHSP70-treated animals because the effects of biological drugs are often attenuated by neutralizing antibody responses (*54*). The treatment of *HexB*$^{-/-}$ mice with rHSP70 induced high levels of serum antidrug antibodies (Fig. 4D).

Table 1. Blood-brain barrier measurements in different regions of mouse brain. The blood-to-brain influx constant (K_{in}) and volume of distribution (V_i) values of ^{3}H-rHSP70 and ^{3}H-albumin for different brain regions after intravenous injection in mice were calculated from the slope and *y* intercept in Fig. 2E.

	K_{in} (ml/g per min)		V_i (µl/mg)	
Brain region	^{3}H-rHSP70	^{3}H-Albumin	^{3}H-rHSP70	^{3}H-Albumin
Whole brain	3.0×10^{-5}	8.8×10^{-6}	0.0178	0.0219
Right and left hemispheres	2.8×10^{-5}	9.3×10^{-6}	0.0174	0.0190
Cerebellum	2.9×10^{-5}	1.0×10^{-6}	0.0225	0.0248
Midbrain	3.9×10^{-5}	1.1×10^{-5}	0.0174	0.0213

rHSP70 attenuates lipid accumulation and disease progression in a murine model of NPC1 disease

Contrary to Fabry disease and Sandhoff disease that are caused by mutations in lysosomal GSL-degrading hydrolases, lipid accumulation

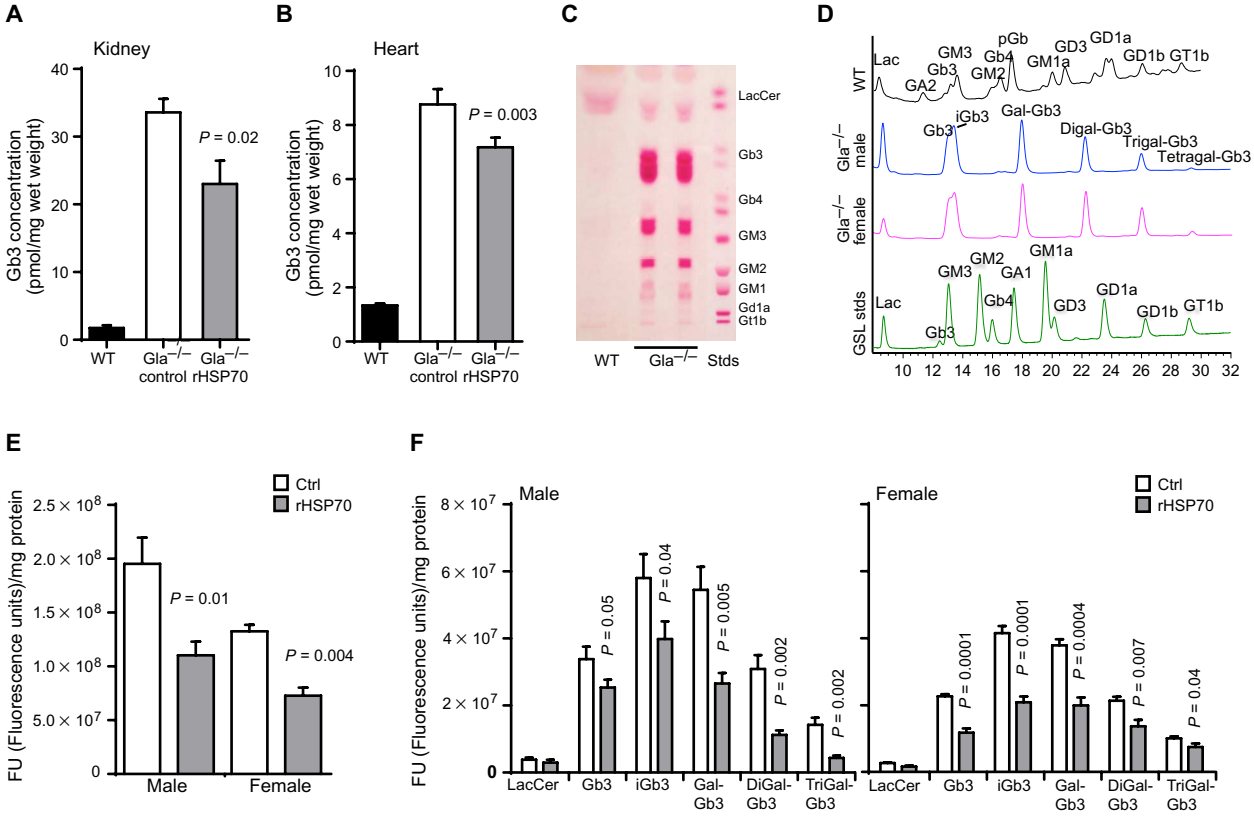

Fig. 3. rHSP70 efficacy in the *Gla*$^{-/-}$ mouse model of Fabry disease. (**A** and **B**) Quantification of Gb3 extracted from kidney (A) and heart (B) of WT, vehicle (PBS) control (*Gla*$^{-/-}$), or rHSP70-treated (*Gla*$^{-/-}$, rHSP70) mice at 17 weeks of age. (**C** and **D**) Analysis of the GSL storage profile of dorsal root ganglia from *Gla*$^{-/-}$ mice by thin-layer chromatography (C) and high-pressure liquid chromatography (HPLC) (D). (**E** and **F**) Quantification of GSL species extracted from dorsal root ganglia of WT, vehicle (PBS) control (*Gla*$^{-/-}$), or rHSP70-treated (*Gla*$^{-/-}$, rHSP70) mice at week 12. *Gla*$^{-/-}$ mice were treated with rHSP70 (5 mg/kg ip) or vehicle (PBS) control, three times per week, from week 3 (after weaning) until euthanasia at 12 weeks of age. Values represent means ± SEM ($n = 4$ to 6 for WT, $n = 5$ to 8 for control *Gla*$^{-/-}$ mice, and $n = 8$ for rHSP70-treated *Gla*$^{-/-}$mice; $P \leq 0.05$). Two-sample comparisons were performed by using Student's *t* test, and multiple comparisons were analyzed by one-way ANOVA followed by Dunnett's multiple comparison test.

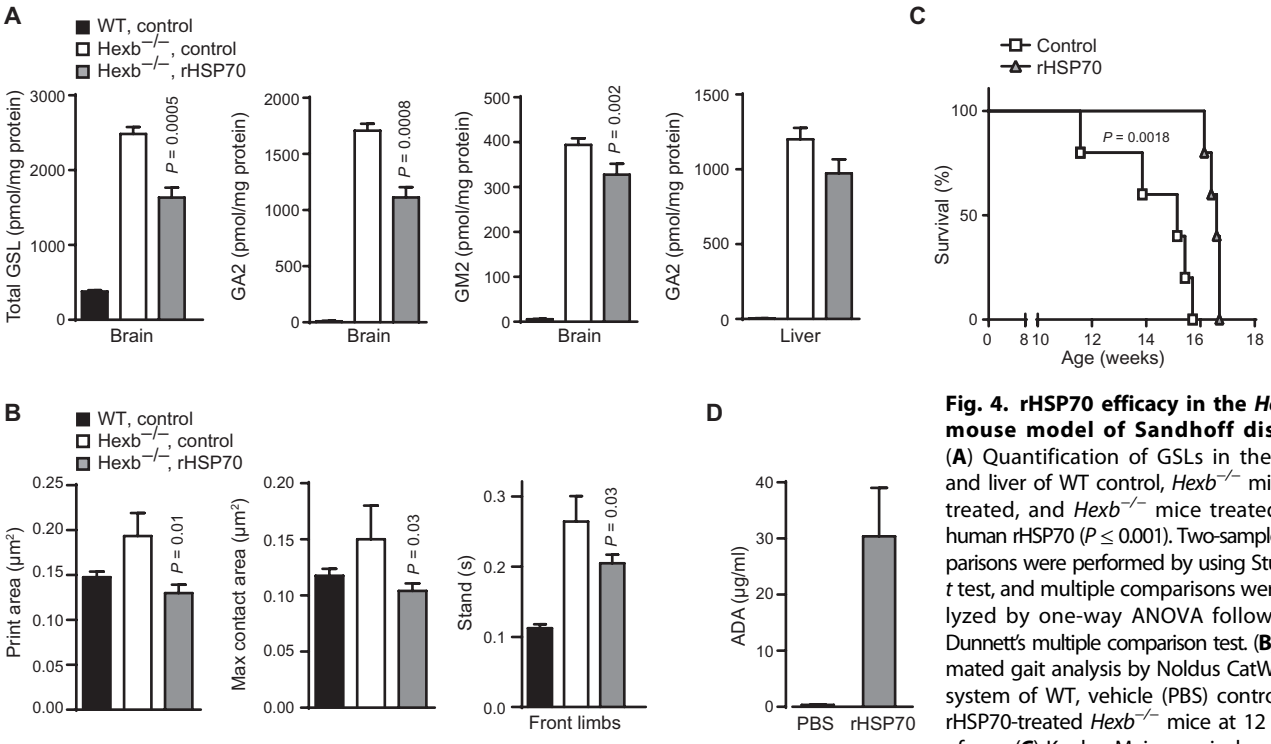

Fig. 4. rHSP70 efficacy in the *HexB*$^{-/-}$ mouse model of Sandhoff disease. (**A**) Quantification of GSLs in the brain and liver of WT control, *Hexb*$^{-/-}$ mice untreated, and *Hexb*$^{-/-}$ mice treated with human rHSP70 ($P \leq 0.001$). Two-sample comparisons were performed by using Student's *t* test, and multiple comparisons were analyzed by one-way ANOVA followed by Dunnett's multiple comparison test. (**B**) Automated gait analysis by Noldus CatWalk XT system of WT, vehicle (PBS) control, and rHSP70-treated *Hexb*$^{-/-}$ mice at 12 weeks of age. (**C**) Kaplan-Meier survival curves of control and rHSP70-treated *Hexb*$^{-/-}$ mice ($P \leq 0.01$). Two-sample comparisons were performed by using Student's *t* test. (**D**) Assay of antidrug antibody (ADA) response. *Hexb*$^{-/-}$ mice were treated with rHSP70 (5 mg/kg ip) or vehicle (PBS) control three times per week from week 3 (after weaning) until euthanasia at week 12 (biochemical analysis) or until reaching the predefined humane end point for survival defined as inability to right themselves when laid on the side. Values represent means ± SEM (n = 10 for behavioral analysis, n = 5 for biochemistry, and n = 5 for survival).

in NPC1 is secondary to defects in endolysosomal transport, which leads to impaired function of lysosomal enzymes such as ASM and responds to treatments that enhance ASM enzyme activity (*39*, *40*). Encouraged by the ability of HSP70 to stimulate ASM activity (*6*, *28*), we studied the effects of rHSP70 on several other lysosomal sphingolipid-degrading enzymes and its ability to reverse lysosomal pathology in NPC1 patient fibroblasts. The murine NPC model used here (*Npc1*$^{-/-}$) replicates some of the biochemical and clinical characteristics of severe infantile/juvenile forms of human NPC disease, such as the accumulation of a broad range of sphingolipids and impaired myelination of the CNS, and also shows progressive ataxia, a hallmark of the human disease (*39*, *64*–*68*). It should, however, be noted that the full therapeutic benefit of rHSP70 could not be properly assessed in this model because HSP70-aided folding of NPC1 protein in the endoplasmic reticulum (ER) could not be assessed in the *Npc1*$^{-/-}$ mice, which have no mutated NPC1 protein (*29*).

Treatment of *Npc1*$^{-/-}$ mice with rHSP70 (3 mg/kg intraperitoneally) three times a week from postnatal day 21 (P21) until euthanasia at P54 reduced the total accumulation of GSLs in the mouse forebrain by 59% (Fig. 5A). It also reduced the accumulation of GSLs in the kidney, liver, and cerebellum and unesterified cholesterol in the kidney and liver (Figs. 2, A to C, and 5A). The reduction of GSL burden was not confined to a single GSL species, but rather all accumulating GSLs measured were reduced after treatment with rHSP70 with the most prominent effects on upstream metabolites of the GSL-catabolic cascade such as gangliosides D1a and T1b (GD1a and GT1b) (Fig. 5A and figs. S2 and S3A). These in vivo data corroborate the in vitro findings of rHSP70's effects on BMP-dependent enzymes and lysosomal pathology in primary fibroblasts from NPC patients (Fig. 1). Impaired myelination is a prominent early pathological feature of NPC and other glycosphingolipidoses, and magnetic resonance imaging analysis of the brains of NPC patients has shown clear correlations between white matter status and neurological symptoms in NPC patients (*2*, *68*–*73*). These clinical observations have been mechanistically supported by observations of decreased expression of myelin gene regulatory factor in the *Npc1*$^{-/-}$ mouse model (*74*). Intriguingly, rHSP70 reduced the cerebral accumulation of GT1b and GD1a, which are involved in myelin regulation (*75*, *76*), by 63 and 58%, respectively ($P \leq 0.01$; Fig. 5A). Administration of rHSP70 also significantly reduced the accumulation of GM1 ganglioside species GM1a, GM1a-gc, and GM1b ($P \leq 0.05$; Fig. 5A and fig. S3), which are mechanistically linked to a neurotoxic unfolded protein response and apoptosis in some LSDs (*77*, *78*). The administration of rHSP70 had an impact on metabolites known to be involved in the regulation of CNS function, particularly myelination. In agreement with these data, rHSP70 significantly increased white matter thickness in the cerebellum and enhanced the levels of myelin basic protein ($P \leq 0.05$; Fig. 5, B and C).

Next, we investigated whether the observed biochemical and histological improvements in myelin in rHSP70-treated *Npc1*$^{-/-}$ mice were also associated with improved motor coordination. Consistent with the biochemical effects of rHSP70 on the CNS and confirming observations from a proof-of-concept study (fig. S2), rHSP70 improved behavioral phenotypes related to cerebellar function (Fig. 5, D to F, and movies S3 and S4). By visual inspection, the treated mice were apparently more

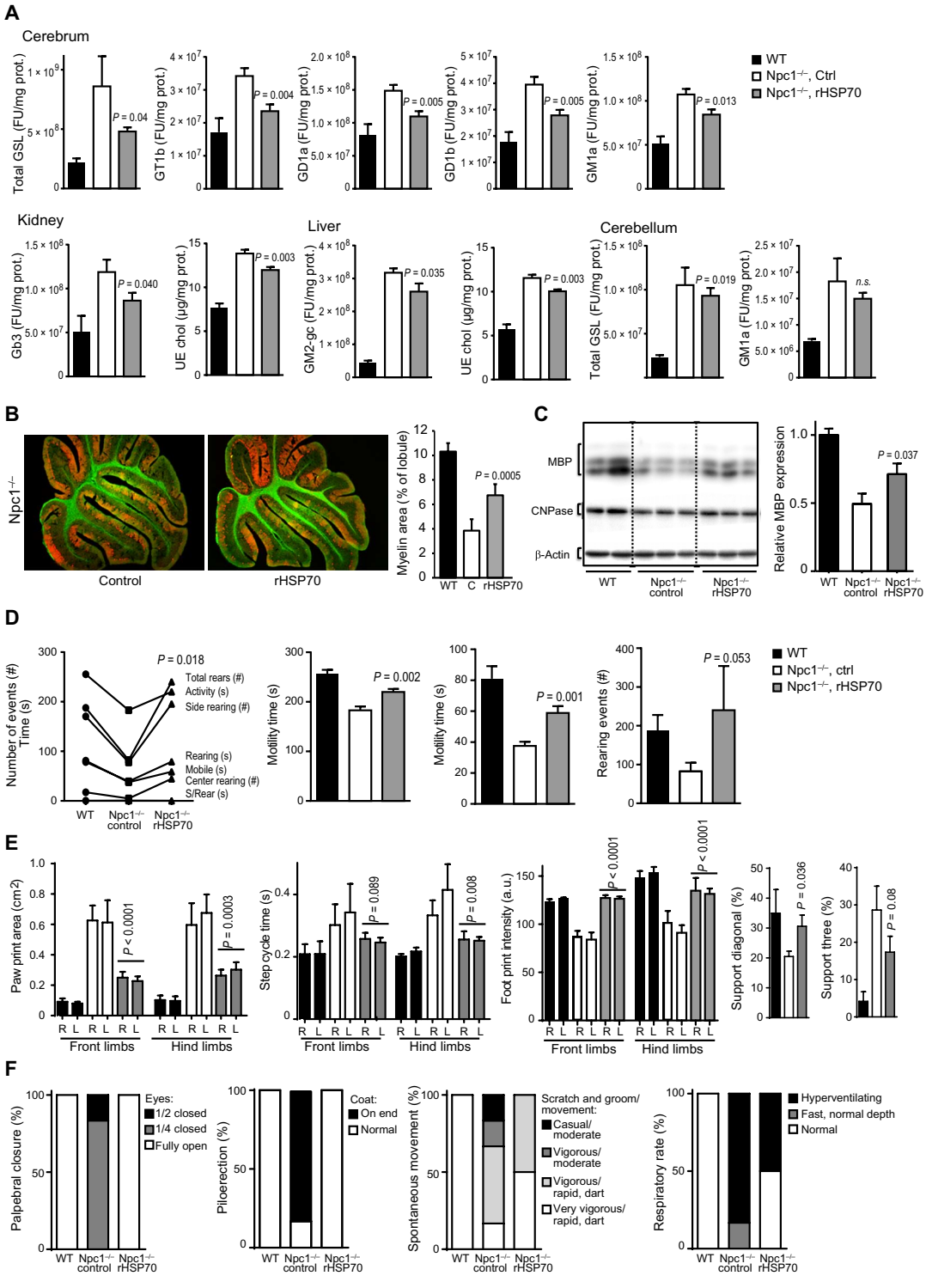

Fig. 5. rHSP70 efficacy in the *Npc1*$^{-/-}$ mouse model of NPC. (**A**) GSL species and unesterified cholesterol extracted from brains, kidney, and liver of WT, vehicle (PBS) control, and rHSP70-treated *Npc1*$^{-/-}$ mice at P54. *Npc1*$^{-/-}$ mice were treated with rHSP70 (3 mg/kg ip) or vehicle (PBS) control three times per week from P21 to P53. Values represent means ± SEM (n = 5 for WT and *Npc1*$^{-/-}$ and n = 6 for rHSP70-treated; $P \leq 0.05$). Two-sample comparisons were performed by using Student's t test, and multiple comparisons were analyzed by one-way ANOVA followed by Dunnett's multiple comparison test. n.s., not significant. (**B**) Representative images and quantifications of cerebellar sections of WT, vehicle (PBS) control, or rHSP70-treated *Npc1*$^{-/-}$ mice at P54 showing Purkinje cells labeled with calbindin (red) and white matter/myelin labeled with cholera toxin (green). Image quantification of myelin content normalized to lobular area is presented in the graph to the right [WT, C (control, PBS-treated), rHSP70 (rHSP70-treated)] (n = 5 to 6; values represent means ± SD). (**C**) Western blot and densitometric quantification of cerebellar MBP expression relative to WT expression normalized to β-actin (n = 4 for WT, n = 5 for *Npc1*$^{-/-}$ control, and n = 6 for rHSP70-treated *Npc1*$^{-/-}$ mice). Values represent means ± SEM. CNPase, 2′,3′-cyclic-nucleotide 3′-phosphodiesterase. (**D**) Automated open-field analysis (AM-Logger system) of behavior of WT (control), vehicle (PBS) control, or rHSP70-treated *Npc1*$^{-/-}$ mice at P47 to P51. *Npc1*$^{-/-}$ mice were treated with rHSP70 (3 mg/kg ip) or vehicle (PBS) control three times per week from P21 (n = 6, values represent means ± SEM; $P \leq 0.05$). Two-sample comparisons were performed by using Student's t test. (**E**) Quantification of automated gait analysis (Noldus CatWalk XT system) of WT (control), vehicle (PBS) control, or rHSP70-treated *Npc1*$^{-/-}$ mice at P49 to P52. *Npc1*$^{-/-}$ mice were treated with rHSP70 (3 mg/kg ip) or vehicle (PBS) control three times per week from P21 (n = 3 for WT, n = 5 for control, and n = 6 for rHSP70-treated). Values represent means ± SEM [$P \leq 0.05$ for all measurements except step cycle (front), P = 0.089 and support (three), and P = 0.08]. Two-sample comparisons were performed by using Student's t test. (**F**) SHIRPA analysis of behavioral and neurological manifestations of disease in WT (control), vehicle (PBS) control, or rHSP70-treated *Npc1*$^{-/-}$ mice at 7 weeks of age. *Npc1*$^{-/-}$ mice were treated with rHSP70 (3 mg/kg ip) or vehicle (PBS) control three times per week from P21 (n = 10 for all groups).

active and better coordinated and had improved coat condition and physical stature (movies S3 and S4). Automated quantification of their activity and coordination in an open-field test confirmed these observations as the rHSP70 treatment significantly improved performance across all measured parameters ($P \leq 0.05$; Fig. 5D). Similarly, automated gait analysis (Noldus CatWalk XT) demonstrated significant rHSP70-induced improvements of the ataxic gait phenotype as measured by a number of disease-specific parameters, such as diagonal support, dual stance, step cycle (hind), paw print area, footprint intensity, base of support, and speed ($P \leq 0.05$; Fig. 5E). These observations were further supported by an independent study using a blinded assessment of the behavioral manifestations of the disease by the SHIRPA (SmithKline Beecham, Harwell, Imperial College, and Royal London Hospital phenotype assessment) test (Fig. 5F). For unknown reasons, the rHSP70-induced antidrug antibody response after 4 weeks of treatment was 8- to 10-fold stronger in the *Npc1*$^{-/-}$ mice than in the wild-type (WT) mice (Fig. 4D and fig. S4B). For this reason, we were not able to perform studies of longer duration in the NPC disease mouse model.

Arimoclomol attenuates lysosomal storage in NPC patient fibroblasts and neurological symptoms in *Npc1*$^{-/-}$ mice

We proceeded to test the efficacy of arimoclomol, an orally available and safe small-molecule HSP70 coinducer with reported efficacy in other neurodegenerative diseases that is currently undergoing clinical testing (*5*, *34*, *35*, *38*, *79*, *80*). This strategy reflects recent reports of the critical role of HSP70 in the maturation of the NPC1 protein (*29*) as well as salvage of the in vitro phenotypes of NPC and other LSDs by up-regulation of HSPs (*27*, *30*, *32*, *81*). Furthermore, the heat shock response has been implicated in a number of chronic neurodegenerative diseases associated with compromised protein function because of genetic alterations (*3*, *4*, *82*).

We began by testing arimoclomol in vitro in primary fibroblasts from NPC patients and in vivo in the *Npc1*$^{-/-}$ mouse model of NPC. Endogenous levels of activated Ser^{326}-phosphorylated HSF1 (pSer^{326} HSF1), the primary transcription factor for HSPs including stress-inducible HSP70, were almost undetectable by Western blotting during unstressed conditions in both WT and NPC1 patient fibroblasts but showed a clear induction upon heat stress (fig. S5A). More sensitive ELISA measurements indicated that HSF1 was only about 50% activated in NPC1 patient fibroblasts compared to healthy control cells (fig. S5B). The very low levels of activated HSF1 during native in vitro growth conditions prompted us to pursue HSF1 activation status and response to arimoclomol in vivo (Fig. 6C). Treatment of NPC1 patient fibroblasts with arimoclomol significantly reduced lysosomal storage and the accumulation of unesterified cholesterol ($P \leq 0.01$ and 0.05; Fig. 6A). A similar reduction in lysosomal accumulation was observed in fibroblasts from patients with NPDA and MLD treated with arimoclomol ($P \leq 0.05$ and 0.001; fig. S6). We next studied the effects of arimoclomol in the *Npc1*$^{-/-}$ mice. Although this model is the best characterized NPC model, it does not replicate the important missense mutations that are the most common type of mutations in NPC and therefore does not allow for the assessment of HSP induction on the folding and maturation of NPC1 protein (*29*). This mouse model, however, did allow us to test whether the therapeutic benefits of HSP70 targeting lysosomal instability could also be achieved with arimoclomol (*6*, *28*). An initial proof-of-concept study demonstrated improvement of ataxia in the NPC mouse model treated with arimoclomol and a 17% increase in survival ($P \leq 0.001$; fig. S7).

We tested arimoclomol in three subsequent experiments using two independent *Npc1*$^{-/-}$ mouse colonies (Fig. 6, B to F) to validate the findings. Characterization of the two colonies revealed that one colony had a slightly more aggressive disease course with earlier onset of ataxia, which provided a larger dynamic range in quantitative gait analysis. Dose-ranging studies indicated that daily oral administration of arimoclomol (10 to 30 mg/kg) was the optimal dose range for reducing ataxic manifestations and behavioral symptoms (Fig. 6B), in line with previously observed efficacious doses for arimoclomol (*5*). Further supported by the reported efficacy of arimoclomol (10 mg/kg) in other preclinical disease models, we chose to focus on this dose (*5*, *38*).

We next analyzed the effect of arimoclomol on Hsf1 activation and Hsp70 levels in brain and liver of *Npc1*$^{-/-}$ mice and healthy mice, in accordance with the proposed mechanism of action of arimoclomol (*5*). Although the liver is biochemically affected in the *Npc1*$^{-/-}$ mouse model, it does not present with the overt hepatomegaly seen with the human early-onset presentation of the disease, so we focused our analysis on brain tissue samples. We observed a reduced amount of activated pSer^{326} HSF1 in the brains of *Npc1*$^{-/-}$ mice, indicating that the *Npc1*$^{-/-}$ mice, despite significant brain pathology, had not mounted a stress response in the CNS (Fig. 6C). This is in line with our in vitro observations (fig. S5) and previous observations of a reduced stress activation level in other animal models of neurodegenerative diseases (*5*, *83*). Analysis of the liver also showed a decrease in activated Hsf1, although less than that observed in the brain (Fig. 6C). Administration of arimoclomol reactivated the stress response in the brains of the treated animals but interestingly did not provide an effect in the liver (Fig. 6C). Both mouse brain and liver had significantly decreased levels of Hsp70, in line with the observed reduced activation state of Hsf1 ($P \leq 0.01$; Fig. 6D). Administration of arimoclomol completely restored Hsp70 levels in the brain but only provided a minor increase in Hsp70 in the liver, consistent with the Hsf1 activation profiles of the two organs (Fig. 6D). The impact on Hsf1 activation and normalization of Hsp70 levels observed in the brain was accompanied by improvements in ataxia ($P \leq 0.01$; Fig. 6E). Furthermore, a separate experiment in which a blinded assessment of neurological and behavioral symptoms (SHIRPA test) was conducted also demonstrated a significant benefit in other neurological manifestations of the disease, such as respiration rate and palpebral (eyelid) closure ($P \leq 0.05$; Fig. 6F). These data demonstrate a neuroprotective effect of arimoclomol treatment in *Npc1*$^{-/-}$ mice (*5*, *38*, *83*).

DISCUSSION

Here, the data presented show that both rHSP70 and arimoclomol reduce biochemical storage levels, improve motor function, and extend life span in several neurological mouse models of LSDs. However, the full effects of these approaches cannot be assessed in knockout models of these diseases as these fail to replicate the essential missense genotypes that constitute most of the mutations in human LSDs, many of which have been shown to be amenable to HSP-based therapies ex situ (*6*, *27*, *29*, *30*, *33*, *84*). We demonstrate the capacity of rHSP70 to augment sphingolipid-degrading enzymes as well as the ability of rHSP70 and arimoclomol to reduce lysosomal accumulation in primary fibroblasts from patients with LSDs. rHSP70 reduced biochemical storage of relevant GSL species in three mouse models of LSDs (Fabry, NPC, and Sandhoff diseases) not only in peripheral organs but also in the CNS of mice with NPC or Sandhoff disease.

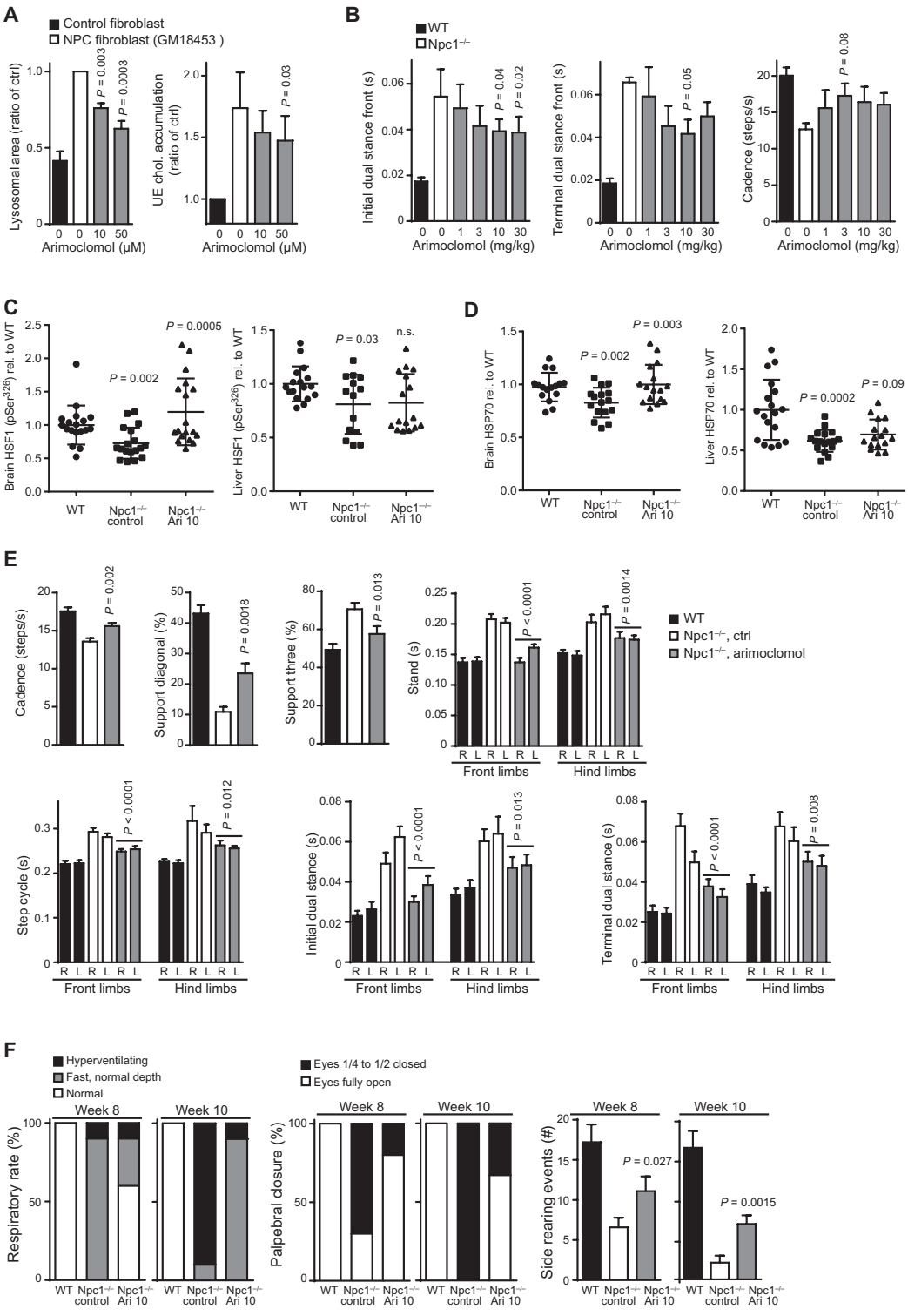

Fig. 6. Arimoclomol treatment and its effects on lysosomal storage and neurological symptoms in the *Npc1*$^{-/-}$ mouse model of NPC. (**A**) Analysis of lysosomal accumulation (left) and storage of unesterified (UE) cholesterol (right) in primary fibroblasts from NPC patients with the I1061T/I1061T haplotype treated with increasing doses of arimoclomol for 24 hours ($P \leq 0.01$ and 0.05, respectively). Data were analyzed by one-way ANOVA followed by Dunnett's multiple comparison test. (**B**) Quantification of automated gait analysis for arimoclomol-treated *Npc1*$^{-/-}$ mice over a dose range of 1 to 30 mg/kg. Mice were administered different concentrations of arimoclomol daily in drinking water from 3 weeks of age until analysis at 7 weeks of age. Values represent means ± SEM ($P \leq 0.05$). Two-sample comparisons were performed by using Student's *t* test, and multiple comparisons were analyzed by one-way ANOVA followed by Dunnett's multiple comparison test. (**C**) Analysis of activated HSF1 (pSer^{326} HSF1) by ELISA in brains and livers of WT, control, or arimoclomol-treated (*Npc1*$^{-/-}$, Ari 10) *Npc1*$^{-/-}$ mice at 7 weeks of age. *Npc1*$^{-/-}$ mice were treated with arimoclomol (10 mg/kg) daily in drinking water or sham (water alone) control from 3 to 7 weeks of age (n = 16 to 18 per group). *P* values denote NPC control versus WT and NPC arimoclomol versus NPC control, respectively. Bars represent average ± SD ($P \leq 0.01$ for brain). Two-sample comparisons were performed by using Student's *t* test. (**D**) Analysis of Hsp70 by ELISA in brains and livers of WT, control, or arimoclomol-treated *Npc1*$^{-/-}$ mice at 7 weeks of age. *Npc1*$^{-/-}$ mice were treated with arimoclomol (10 mg/kg) daily in drinking water or sham (water only) as control from 3 to 7 weeks of age (n = 16 to 18 per group). *P* values denote NPC control versus WT and NPC arimoclomol versus NPC control, respectively. Bars represent average ± SD ($P \leq 0.01$ for brain). Two-sample comparisons were performed by using Student's *t* test. (**E**) Quantification of automated gait analysis of WT, control, or arimoclomol-treated *Npc1*$^{-/-}$ mice at 7 weeks of age. *Npc1*$^{-/-}$ mice were treated with arimoclomol (10 mg/kg) daily in drinking water from 3 to 7 weeks of age or sham (water only) control. Values represent mean ± SEM (n = 10 per group; $P \leq 0.01$). Two-sample comparisons were performed by using Student's *t* test. (**F**) SHIRPA analysis of behavioral and neurological manifestations of disease in WT, control, or arimoclomol-treated *Npc1*$^{-/-}$ mice at 7 weeks of age. *Npc1*$^{-/-}$ mice were treated with arimoclomol (10 mg/kg) daily in drinking water or sham (water only) control from 3 to 10 weeks of age (n = 10 per group).

The effect of rHSP70 on GSL species involved in myelination, and neuronal survival provided new insights into potential mechanisms for the neuroprotective and cytoprotective effects of HSP70 (*4*, *11*, *85*, *86*). The mechanism of action and the biochemical and behavioral responses in the two neurological mouse models of LSDs clearly distinguish HSP70-based therapies from other LSD therapeutic approaches (*54*, *64*, *87*–*90*). Although the NPC1$^{-/-}$ mouse model still retains functional, albeit compromised, sphingolipid-degrading enzymes that can be directly augmented by rHSP70 (*6*, *28*), the effects of rHSP70 in the Fabry and Sandhoff disease mouse models cannot be explained by a direct effect on the missing enzymes. However, studies of substrate reduction therapies in both models have demonstrated that secondary metabolic pathways exist, as blockade of substrate synthesis by glucosylceramide synthase inhibitors, such as miglustat, leads to reduction of substrate storage levels in both diseases (*61*, *63*). It is thus conceivable that the effects of rHSP70 are mediated by its interaction with other sphingolipid-metabolizing enzymes such as GLB, which has previously been shown to have effects on Gb3 (*91*). Given the broad capacity of rHSP70 to improve the function of GSL-degrading enzymes and its effects on endolysosomal trafficking, it is likely that the effects observed may be mediated through an increase in the activity of these pathways, potentially through a mechanism similar to that for HSP70's effect on ASM activity (*6*, *13*, *23*, *28*), although this requires further investigation.

We investigated the orally available small-molecule HSP coinducer, arimoclomol. This molecule is currently being evaluated in late-stage clinical studies of other neurodegenerative diseases, such as familial amyotrophic lateral sclerosis (ALS) and sporadic inclusion body myositis (sIBM), and therefore has a human clinical safety record, making it an ideal candidate for potential chronic use in LSDs (ClinicalTrials.gov identifiers NCT00706147 and NCT00769860) (*5*, *33*–*35*, *38*, *54*, *79*, *80*). Contrary to other HSP inducers, arimoclomol does not stress the cell but instead acts as a coinducer of HSPs, particularly HSP70 (*3*, *5*, *37*). Its described mechanism of action involves binding to and stabilizing the interaction of HSF1 with HSEs, the transcriptional elements controlling HSP production (*5*, *36*). By facilitating the production of HSPs in this way, arimoclomol does not in itself stress cells or lead to the direct induction of HSPs, which is dissimilar to other HSP-inducing agents such as vorinostat (SAHA) and Velcade (bortezomib) (*81*, *84*). Akin to the direct administration of rHSP70, arimoclomol provided a disease-relevant response in patient-derived primary fibroblasts harboring the most common NPC1 allele (I1061T) (*92*). This is in line with a recent report by Nakasone *et al.* (*29*) describing a critical role for HSP70 in the proper folding and trafficking of the NPC1 protein.

Analysis of the stress response in the *Npc1*$^{-/-}$ mouse model revealed that the activation of Hsf1, a critical transcription factor for HSP production, was attenuated, even in the pathologically most severely affected organ, the brain, and that it could be reactivated by administration of arimoclomol. Crucially, the reactivation of Hsf1 and normalized Hsp70 expression in the brain of *Npc1*$^{-/-}$ animals were paralleled by clear improvements in all measured neurological phenotypes. Arimoclomol demonstrated a clear effect on the clinically most relevant end points in the *Npc1*$^{-/-}$ mouse model, as all 13 ataxic gait parameters measured using the CatWalk automated system as well as respiration measured by blinded neurological examination (SHIRPA) were significantly improved. This is encouraging because reduced motor coordination and ataxia are cardinal clinical symptoms of NPC and because reduced diaphragm function and associated illnesses constitute significant morbidities in NPC patients (*65*, *93*).

Although the full potential of arimoclomol cannot be addressed in the *Npc1*$^{-/-}$ mouse model because it is null and does not replicate the missense mutations found in most patients, we still observed that the effects of arimoclomol were similar to the responses observed with rHSP70, indicating that arimoclomol provides the same benefits as the administration of the recombinant protein in this model, which are independent of the presence of the NPC1 protein. A potentially relevant NPC1 mouse model carrying the missense mutation (I1061T) was recently reported and might provide a model for future testing of HSP-based strategies, pending its thorough characterization and evaluation as a relevant preclinical model (*94*).

Our data suggest that rHSP70 is a feasible candidate for clinical development even for treating chronic diseases, although antibody reactions to human proteins are a well-known challenge within the LSD field (*54*). In this regard, it is important to note that patients are not immunologically naïve to HSP70 as is the case for some enzyme replacement therapies and that rHSP70 has been shown to be safe even after 9 months of dosing in mice (*95*). Notably, a constitutive increase of HSP70 as exemplified in transgenic animals overexpressing HSP70 does not have any effects on development as these animals develop normally; these animals are protected from ischemia and reperfusion injuries to the myocardium (*96*, *97*).

Even so, compared to lifelong intravenous administration of a recombinant protein, small-molecule HSP inducers would be predicted to be a superior option for patients provided that they are safe and suited for chronic use. Most existing HSP inducers stress cells because of their various toxic effects, which makes their chronic use undesirable (*33*). We therefore used a small-molecule arimoclomol, which has undergone seven phase 1 safety trials and three phase 2/3 clinical trials for ALS and sIBM, where it has a demonstrated safety profile compliant with chronic use (ClinicalTrials.gov identifiers NCT00706147 and NCT00769860) (*34*, *35*, *98*).

The ability of arimoclomol to reactivate HSF1 in the brains of *Npc1*$^{-/-}$ mice as well as the role of HSP70 in sphingolipid degradation in three models of sphingolipidoses suggest the potential of HSP-based therapeutics for treating these diseases. In addition, the reported cytoprotective roles of HSPs, in particular HSP70 in lysosomes, and the role of HSP70 in the folding and trafficking of NPC1, glucocerebrosidase, and NEU support the notion that sphingolipidoses might present a therapeutic opportunity for HSP-based therapies (*6*, *28*, *29*). HSP-based therapies mediate their effects through multiple independent mechanisms of action, reflecting the multiple biological roles of the HSP70 system (*33*).

Although the strength of the HSP system lies in its multifaceted cytoprotective actions, there are also potential limitations because it is challenging to discern which pathway is the most critical for potential clinical efficacy. This challenge is exacerbated by the fact that most sphingolipidoses are relatively poorly characterized, with their molecular etiology often obscure (*99*, *100*). The mouse models used in this study are the best characterized for each disease, but they are lacking one of the most important features of LSDs, which is the presence of missense mutations and the associated misfolding of enzymes. These animal models lack not only a fundamental part of the human disease but also the capacity for testing the ability of HSP-based strategies to regulate folding in the ER and relieve ER-associated stress and the unfolded protein response (*101*).

Another challenge to developing HSP-based therapies is that of dose translation from preclinical models to human patients. For example, the level of HSP induction required for the best clinical response is not known. The dynamic range of the HSP system and, in particular, induction of HSP70 is large and is variable depending on the stressor, the amount of exposure, what tissue is being studied, etc. Drugs often used in HSP experiments such as proteasome inhibitors, HSP90 inhibitors, and histone deacetylase inhibitors provide high induction of HSPs but are also cytotoxic. Although they can be used to demonstrate principles, it is clear that drugs that provoke HSP induction through toxic actions are poorly suited for chronic use. For these reasons, we investigated the small-molecule arimoclomol, which provides a more subtle and less aggressive manipulation of the HSP system and has been demonstrated to be safe in both animal models and human patients. Arimoclomol belongs to a family of drugs that have demonstrated effects across a number of animal models of neurodegenerative diseases (*7*, *8*, *37*). Arimoclomol has demonstrated potential therapeutic benefits in several animal models of neurological and motor neuron disorders, including ALS, Kennedy's disease (spinobulbar muscular atrophy), acute injury–induced neuronal death, and sIBM, as well as in retinitis pigmentosa and diabetic peripheral neuropathy and retinopathy (*5*, *38*, *83*, *102*–*104*). In addition, arimoclomol has been demonstrated to enter the CNS efficiently and to be safe and well tolerated in a number of clinical trials (*34*, *35*, *98*). Arimoclomol is currently being tested in a phase 2/3 randomized, double-blind, placebo-controlled trial in patients with familial ALS due to mutations in superoxide dismutase 1 (NCT00706147).

It remains to be demonstrated whether these encouraging effects with arimoclomol translate into clinical efficacy for ALS and sIBM (*34*, *98*). Optimal dosing and duration of dosing are clear limitations in both studies and will have to be carefully evaluated in future clinical trials to ensure the best study design to demonstrate both safety and efficacy. In this regard, sphingolipidoses are challenging because validated biomarkers only exist for a few of these diseases. However, the emerging convergence of mechanisms between the sphingolipidoses and the HSP system provides an opportunity to develop new biomarkers for assessing responses to drug therapy (*33*).

Our study suggests that HSP-based strategies may have therapeutic potential for treating sphingolipidoses. In particular, we demonstrate that rHSP70 and arimoclomol present two attractive clinical candidates for treating the neurological symptoms of sphingolipidoses including NPC with arimoclomol currently in a phase 2/3 clinical trial in NPC patients (ClinicalTrials.gov identifier NCT02612129).

MATERIALS AND METHODS

Study design

The design of this study aimed to address whether the mechanism of HSP70-based lysosomal functional improvement, which we have previously published, could be extended to encompass several different sphingolipidoses. The study further sought to address critical components of translational drug development for a recombinant protein such as safety, distribution, CNS penetrance, and efficacy. Finally, the study asked whether the same benefits observed with rHSP70 could be achieved with arimoclomol, a clinically well-tolerated, orally available small-molecule HSP amplifier. We studied the effects of rHSP70 and arimoclomol in several different in vitro, ex situ, and in vivo models including well-characterized animal models of several sphingolipidoses.

Initial studies included assessment of protein/lipid interactions in lipid membrane bilayers followed by testing of biological activity in primary cells from patients suffering from different sphingolipidoses. We then analyzed the pharmacological properties of rHSP70 through in vitro and in vivo safety, PK, and distribution studies. Efficacy was tested in vitro and in vivo in three independent mouse models of sphingolipidoses: Fabry disease, Sandhoff disease, and NPC.

Arimoclomol was tested in vitro and in vivo in two independent mouse colonies modeling NPC. Powering of the studies was based on previous publications of variance in measurements in the in vitro and in vivo studies and a characterization study performed on the second independent colony of NPC mice before dose range–finding experiments. All in vitro experiments were repeated in at least three independent cultures. For in vivo studies, mice were assigned randomly in all studies and handled according to National and Institutional Animal Care and Use Committee guidelines. In vivo efficacy experiments were conducted blind to treatment. Figure legends include details of replicate experiments used to generate data sets.

Cells

LSD fibroblasts (GM02769, GM00881, GM02921, GM06806, GM04372, GM10915, GM00197, GM02093B, GM17918, GM18453, and GM18414) and control fibroblasts (GM02770, GM02922, GM06808, GM00200, and GM05659) were obtained from the Coriell Cell Repository. NPDA primary fibroblast B534 R496L was a gift from E. Schuchman. Farber disease primary fibroblasts 89/78 and 89/73 were a gift from K. Sandhoff. All cells were grown at 37°C with 5% CO_2 in Dulbecco's modified Eagle's medium with 12% fetal calf serum, nonessential amino acids, and 1% penicillin-streptomycin. Treatment with recombinant human His-tagged HSP70 and measurement of lysosomal accumulation were performed as previously described (*6*). For A2M competition experiments, cells were seeded in Nunc Lab-Tek four-well chambered coverglass. Twenty-four hours later, cells were given one of the following three treatments: pretreatment with 142 nM A2M (Sigma-Aldrich) on ice for 30 min followed by 1.42 μM A2M + 286 nM rhHSP70-AF488 for 1 hour at 37°C, no pretreatment but also 30 min on ice followed by 286 nM rhHSP70-AF488 for 1 hour at 37°C, or pretreatment with A2M (100 μg/ml) on ice for 30 min followed by 1.42 μM A2M for 1 hour at 37°C (negative control). Medium was removed, and PBS (+/+) with 3% fetal bovine serum was added. Eight pictures were taken per condition, and area of green fluorescence (HSP70-AF488 uptake) per cell number was calculated. A minimum of 100 cells was measured per repetition of the experiment.

Recombinant HSP70

rHSP70 was manufactured as described previously (*6*), with protocols for good laboratory practice and good manufacturing practice production amended to meet the requirements to large-scale manufacture. All batches were produced and controlled according to regulatory guidelines for biological products with, for example, endotoxin concentrations <5 endotoxin units/mg.

Animal studies

All animal studies were approved by the U.K. Home Office for the conduct of regulated procedures under license (Animal Scientific Procedures Act, 1986), were conducted in strict accordance with the

National Institutes of Health (NIH) *Guide for the Care and Use of Laboratory Animals* guidelines, were in accordance with Dutch law, and were approved by the Animal Care and Use Committee of the University of Groningen, Netherlands.

Liposome-bead assay

To prepare the liposomes, we used different lipids: 1.4 mM sphingomyelin, 50 mM phospatidylcholine, 2.6 mM cholesterol, and 6.31 mM BMP. After evaporation of the solvent, the mixture was resuspended in 500 μl of 2 mM tris-HCl (pH 7.4), vortexed thoroughly for 1 min, subjected to six freeze and thaw cycles in liquid nitrogen and 37°C incubator, and vortexed again for 1 min. The suspension was afterward put through a polycarbonate membrane using Mini Extruder (Avanti Polar Lipids Inc.) for at least 20 times. The freshly made liposomes were mixed in a 1:1 ratio with magnetic silica (MoBiTec) or silica beads (Bangs Laboratories) and incubated for 1 hour at room temperature. Afterward, the beads were separated from the unbound liposomes using centrifugation at 12,000*g* for 1 min for silica beads or using the separator for magnetic silica beads. The beads were washed with 0.5× PBS and resuspended in the same amount of 0.5× PBS buffer as the 1:1 mixture of liposomes and beads. The resuspended beads were stored at 4°C.

The analyzed proteins were labeled with AF488 using the Microscale Protein Labeling Kit (Life Technologies) according to the provided protocol. The labeled proteins were diluted to reasonable numbers during fluorescence detection (3000 to 10,000 refractive indices) using 100 mM acetate buffer solution (pH 4.5). HSP70 was stored in PBS buffer and diluted to various concentrations used in the assay in 100 mM acetate buffer solution (pH 4.5).

For the assay, 10 μl of the labeled protein dilution was mixed with 10 μl of beads and 10 μl of acetate buffer solution or HSP70 dilution, mixed carefully up and down with a pipette, and incubated and protected from light for 1 hour at room temperature. Afterward, the beads were separated carefully from the liquid phase using centrifugation at 12,000*g* in the tabletop centrifuge for 5 min and room temperature for silica beads (Bangs Laboratories) or using the magnetic separator for magnetic silica beads (MoBiTec). Liquid phase (25 μl) was mixed with 75 μl of 2 mM tris-HCl (pH 7.4) and transferred to a 96-well plate for fluorescence measurement using the PerkinElmer 2030 plate reader with light absorption at 480 nm, emission at 520 nm, and counting times of 0.1 to 0.2 s. The equilibrium between protein bound to beads and protein in solution was adjusted, so about two-thirds of the protein was unbound (in solution) in the absence of HSP70. Analysis of the decrease of protein in solution and the simultaneous increase in binding to the lipid beads in response to increasing rHSP70 was then performed. In a typical experiment, the amount of protein in solution decreased by up to 30% at increasing concentrations of rHSP70, whereas the protein bound to the beads increased up to 50%. The significance of the values obtained by this assay was in most cases high to very high. For quenching measurements, 10 μl of the labeled protein dilution alone and the mixture of 10 μl of labeled protein dilution and 10 μl of HSP70 dilution were mixed with 90 and 80 μl of 2 mM tris-HCl (pH 7.4), respectively, and transferred to a 96-well plate for fluorescence measurements.

Bioanalysis of rHSP70, PK, and distribution

The concentration of rHSP70 in plasma and tissues was measured by ELISA (ADI-EKS-715 or ADI-EKS-700B, Enzo Life Sciences) and autoradiography using a gamma counter (Cobra II) for studies of ^{125}I-rHSP70. The studies were performed in 54 outbred male mice from Taconic Europe A/S. All animal studies were approved by Dyreforsøgstilsynet (Denmark) and carried out in accordance with the NIH *Guide for the Care and Use of Laboratory Animals* guidelines. At the start of the acclimatization period, the mice were 5 to 6 weeks old. An acclimatization period of at least 5 days was allowed to reject animals in poor condition or at the extremes of the weight ranges. The animals were dosed either intravenously or intraperitoneally with ^{125}I-rHSP70 (1 to 50 mg/kg) as stated in the figure text. Blood sampling for toxicokinetic calculations was performed at the following time points: 5, 15, 30, 60, 120, and 360 min after treatment. For distribution analysis, tissue samples were collected and saline-perfused. Samples were measured using a gamma counter (Cobra II) and bioanalysis (ELISA) according to the manufacturer's instructions.

Toxicokinetic calculations

Mean plasma concentration profiles were subjected to noncompartmental PK analysis using the PC-based software WinNonlin Professional version 5.2.1 by Pharsight Corporation. A noncompartmental analysis using WinNonlin model 200 (extravascular bolus dose model) and model 201 (intravenous bolus model) was performed.

After C(0) had been reached, concentrations below lower limit of quantification (LLOQ) were entered as half the value of LLOQ ($^1/_2$ * LLOQ). Data points below LLOQ followed by another data point below LLOQ were excluded from modeling and analysis.

Evaluation of rHSP70 PK in adult rat brain

Adult male Wistar rats (262 to 293 g; Charles River) were used for the experiment. The experiment was conducted in strict accordance with the NIH *Guide for the Care and Use of Laboratory Animals* guidelines, was in accordance with Dutch law, and was approved by the Animal Care and Use Committee of the University of Groningen, Netherlands. Surgery, microdialysis probe implantation, femoral vein cannulation, and sampling were performed as previously described (*105*). rHSP70 (1.2 mg/ml) was administered intravenously by infusion through the femoral vein cannula at a rate of 1 ml/kg per min. Bioanalysis of microdialysis samples was performed as described herein. Brain homogenization and capillary spin-down were performed as previously described (*46*). Bioanalysis of brain tissue samples was performed as described herein.

Blood-to-brain influx constant measurements

rHSP70 was labeled with tritium using the method described by Begley and Chain (*106*) scaled down for small quantities of protein. Measurement and analysis of the influx constant of ^{3}H-rHSP70 were performed as previously described (*47*) with the following experimental regimen: female C57B6 mice were used at 7 to 8 weeks of age. The mice had free access to food and water and were maintained on a 12-hour dark/light cycle in a room with controlled temperature (24 ± 1°C) and humidity (55 ± 5%). Mice were anesthetized with Avertin (20 ml/kg of 1.2% solution) before they receive an intravenous injection of ^{3}H-HSP70 (average 20 mg/kg) or ^{3}H-albumin (average 16 mg/kg) into the jugular vein. At 1, 3, 5, 10, 15, 20, 30, and 60 min after the injection, mice were killed with an overdose of Avertin. Blood was collected from the chest cavity after opening of the thorax and heart, and the brain was dissected into four main regions (right, left, midbrain, and cerebellum). After the centrifugation of blood samples, 50 μl of plasma was added to 500 μl of

solubilizer (Solvable) for 24 hours at 37°C. Tissues were weighed and also left to dissolve in 500 μl of solubilizer (Solvable) for 24 hours at 37°C. At the end of this period, 4.5 ml of liquid scintillation cocktail (Ultima Gold) was added and the vials were counted in the scintillation counter.

Antidrug antibody assay

We developed an ELISA for the determination of a potentially neutralizing immunoglobulin G (IgG) response after administration of rHSP70 and used this to determine the presence of anti-HSP70 in serum from rHSP70-treated and rHSP70-untreated mice. The primary anti-HSP70 antibody was from Assays Design (1 mg/ml; catalog no. C92F3A-5), and secondary horseradish peroxidase (HRP)–conjugated anti-mouse IgG was from Bethyl Laboratories (Goat x-mouse IgG-Fc HRP-conjugated, from Mouse IgG ELISA Quantitation Set, catalog no. E90-131, lot no. E90-131-27). The substrate was TMB One Ready-to-use substrate (Kem-En-Tec Diagnostics), and the coating buffer was 0.05 M carbonate-bicarbonate (pH 9.6). ELISA blocking buffer contained 50 mM tris + 0.14 M NaCl + 1% bovine serum albumin (BSA) (pH 8.0).

ELISA wash buffer contained 50 mM tris + 0.14 M NaCl + 0.05% Tween 20; Sample/Conjugate Diluent contained 50 mM tris + 0.14 M NaCl + 1% BSA, 0.05% Tween 20; and ELISA Stop Solution contained 1 M HCl. Briefly, plates were coated with 50 μl of diluted antigen (20 μg/ml) for 60 min at 25°C or overnight at 4°C. The plates were then washed and blocked for 30 min at 25°C. Appropriately diluted samples (50 μl) and a reference standard antibody were then incubated for 60 min at 25°C, the plates were washed, and substrate was added. The reaction was stopped with 50 μl of 1 M HCl, and absorbance was measured at 450 nm. The concentration of antibody in the sample was calculated on the basis of the standard reference.

Npc1$^{-/-}$ mouse model

BALB/cNctr-*Npc1*^{m1N}/J (The Jackson Laboratory) mice (termed NPC1$^{-/-}$ mice, also known as NPC^{nih} mice) were maintained by heterozygote brother/sister mating and genotyped as previously described (Loftus, 1997; #516) (*107*). Mice were group-housed in ventilated cages with irradiated food and bedding and autoclaved water available ad libitum. WT mice were NPC$^{+/+}$ generated from the same litters as the NPC1$^{-/-}$ mice. All animal studies were approved by the U.K. Home Office for the conduct of regulated procedures under license (Animal Scientific Procedures Act, 1986). Three-week-old NPC1$^{-/-}$ mice were treated with recombinant human His-tagged HSP70 at 3 mg/kg (NPC1$^{-/-}$ + rHSP70; $n = 6$) of body weight or with PBS (NPC$^{-/-}$ control; $n = 6$). Mice were injected three times per week intraperitoneally. WT BALB/c mice were used as baseline controls ($n = 6$). Mice were killed at 54 days of age. For biochemical analysis, mice were killed by asphyxiation in rising concentrations of CO_2 and perfused through the left cardiac ventricle with ice-cold PBS. Tissues were homogenized in ice-cold PBS. For immunofluorescence, mice were killed by asphyxiation in rising concentrations of CO_2 and perfused through the left cardiac ventricle with ice-cold 4% paraformaldehyde (PFA). Brains were removed whole and left overnight in 4% PFA before being transferred to 30% sucrose in PBS at 4°C.

Immunofluorescence

Cryoprotected cerebellums were sectioned parasagittally at 30 μm and stored at −20°C in a glycerol/ethylene glycol storage solution. Before staining, sections stored at −20°C were left for 30 min at room temperature and were then washed three times in PBS. Sections were incubated in wells overnight at 4°C with mouse anti-calbindin antibody (Swant, catalog no. 300) made up in PBS with 0.5% Triton X-100 and 2% normal goat serum. Secondary antibodies (DyLight 594 anti-mouse) were made up in PBS with 0.5% Triton X-100 and 2% normal goat serum and were incubated for 2 hours at room temperature. Cholera toxin B subunit directly conjugated to AF488 (Invitrogen, catalog no. C-34775) was used at 1:500 in PBS with 0.5% Triton X-100 and 2% BSA. Sections were incubated overnight at 4°C. All washing steps were performed three times in PBS. Sections were mounted onto Superfrost slides and allowed to air dry overnight protected from light and dust before mounting in Mowiol. Images of lobules IV and VI (early and late degenerating lobules, respectively) were obtained using a Zeiss fluorescence microscope and Zeiss AxioVision camera and software. Measurements of myelin area and length were performed with ImageJ software (version 1.46r; NIH).

Western blotting

Brain homogenates were stored with 1% Igepal CA, 0.5% sodium deoxycholate, 0.1% SDS, and 1% protease inhibitor cocktail (Sigma-Aldrich, catalog no. P-8340). Samples were resolved using 12% SDS–polyacrylamide gel electrophoresis and transferred to nitrocellulose membrane (Bio-Rad) using semidry transfer apparatus. MBP was probed with SMI-94 antibody (Cambridge Bioscience) and β-actin antibody (Sigma-Aldrich, a3854), and immunoreactivity was detected using Amersham ECL substrate (GE Healthcare, RPN2232).

Enzyme-linked immunosorbent assay

HSF1 (ADI-900-199 from Enzo) and HSP70 (ADI-EKS-700B from Enzo) ELISAs were performed on 200 μg of protein according to the manufacturer's instructions.

GSL and cholesterol measurement

All GSL measurements were performed via ultra-HPLC analysis as previously described (*108*). Cholesterol was extracted from the relevant tissues using a modified Folch extraction method (*109*). Briefly, samples were adjusted to protein content (0.5 mg/ml) in double-distilled water (ddH_2O) and extracted in 20 volumes of 2:1 chloroform/methanol for 2 hours at room temperature. After extraction, four volumes of methanol were added and samples were centrifuged to remove insoluble material. To the retained supernatant, chloroform and water were added to achieve a final ratio of 8:4:3 chloroform/methanol/water. After centrifugation, the upper phase was removed by pipetting, and the lower phase was washed three times with 3:48:47 chloroform/methanol/water. Washed lower phase containing cholesterol was dried under N_2. All extraction steps were performed in borosilicate glass.

We quantified unesterified cholesterol with the Amplex Red Molecular Probes kit according to the manufacturer's instructions. Briefly, extracted samples were resuspended in 1× reaction buffer (supplied) at a concentration equivalent to protein (0.5 mg/ml). Sample (50 μl) was loaded into a 96-well plate in triplicate alongside a cholesterol reference standard (0 to 20 μg). For the reaction to measure free cholesterol, an equal volume of 1× reaction buffer containing 150 μM Amplex Red, HRP (1 U/ml), and cholesterol oxidase (1 U/ml) was added to the wells. The plate was then incubated for 30 min at 37°C. Fluorescence was analyzed using a FLUOStar Optima plate reader (BMG Labtech) (excitation, 560 ± 10 nm; emission, 590 ± 10 nm). For cell cultures, cholesterol was quantified with the Amplex Red Molecular

Probes kit as described above and by preparing cultured fibroblast samples through harvest of cells in ddH_2O and sonication at high intensity using a Diagenode Bioruptor.

Open-field analysis

We performed open-field analysis as described previously (*110*). Briefly, mice were placed in "open field" for 5 min. Activity was recorded using the AMLogger with Activity Monitor software AM1053 (Linton Instruments).

Manual rearing

Mice were placed in a large open-field cage box for 5 min. A side rear was recorded when mice reared on hind legs using the side of the cage as support. A center rear was recorded when mice reared on hind legs unaided. Rearings that were uncontrolled/the mouse fell over were discounted.

Gait analysis

Gait analysis was performed using the CatWalk system (Noldus). Mice were filmed walking three times across a backlit stage at weekly intervals. Footprint and stride measurements from the longest continuous set of uninterrupted motion in each of the three walks were assigned and analyzed using the CatWalk XT software v9.1 (Noldus).

Statistical analyses

All statistical analyses were performed with GraphPad Prism software (version 6.02). Two-sample comparisons were performed using Student's *t* test, and multiple comparisons were analyzed by one-way ANOVA followed by Dunnett's multiple comparison test.

SUPPLEMENTARY MATERIALS

www.sciencetranslationalmedicine.org/cgi/content/full/8/355/355ra118/DC1

Fig. S1. rHSP70 uptake in NPC patient fibroblasts and lymphocytes.

Fig. S2. rHSP70 in $Npc1^{-/-}$ mouse model pilot study and manual behavior quantification.

Fig. S3. GSL and behavioral analyses of rHSP70-treated $Npc1^{-/-}$ mice.

Fig. S4. Antidrug antibody responses against rHSP70.

Fig. S5. In vitro analysis of activated HSF1 ($pSer^{326}$ HSF1).

Fig. S6. Effect of arimoclomol on lysosomal accumulation in NPDA and MLD.

Fig. S7. Arimoclomol increases survival of $Npc1^{-/-}$ mice.

Fig. S8. Plasma and thyroid gland distribution of ^{125}I-rHSP70.

Movie S1. Uptake and effect of rHSP70 on the endolysosomal system in NPD primary patient fibroblasts.

Movie S2. Endolysosomal dynamics in NPD primary patient fibroblasts.

Movie S3. Video of gait analysis of PBS-treated control $Npc1^{-/-}$ mice.

Movie S4. Video of gait analysis of rHSP70-treated $Npc1^{-/-}$ mice.

REFERENCES AND NOTES

1. G. Parenti, G. Andria, A. Ballabio, Lysosomal storage diseases: From pathophysiology to therapy. *Annu. Rev. Med.* **66**, 471–486 (2015).
2. Y.-H. Xu, S. Barnes, Y. Sun, G. A. Grabowski, Multi-system disorders of glycosphingolipid and ganglioside metabolism. *J. Lipid Res.* **51**, 1643–1675 (2010).
3. D. W. Neef, A. M. Jaeger, D. J. Thiele, Heat shock transcription factor 1 as a therapeutic target in neurodegenerative diseases. *Nat. Rev. Drug Discov.* **10**, 930–944 (2011).
4. P. J. Muchowski, J. L. Wacker, Modulation of neurodegeneration by molecular chaperones. *Nat. Rev. Neurosci.* **6**, 11–22 (2005).
5. D. Kieran, B. Kalmar, J. R. T. Dick, J. Riddoch-Contreras, G. Burnstock, L. Greensmith, Treatment with arimoclomol, a coinducer of heat shock proteins, delays disease progression in ALS mice. *Nat. Med.* **10**, 402–405 (2004).
6. T. Kirkegaard, A. G. Roth, N. H. T. Petersen, A. K. Mahalka, O. D. Olsen, I. Moilanen, A. Zylicz, J. Knudsen, K. Sandhoff, C. Arenz, P. K. J. Kinnunen, J. Nylandsted, M. Jäättelä, Hsp70 stabilizes lysosomes and reverts Niemann-Pick disease-associated lysosomal pathology. *Nature* **463**, 549–553 (2010).
7. L. Vígh, P. N. Literáti, I. Horváth, Z. Török, G. Balogh, A. Glatz, E. Kovács, I. Boros, P. Ferdinándy, B. Parkas, L. Jaszlits, A. Jednákovits, L. Korányi, B. Maresca, Bimoclomol: A nontoxic, hydroxylamine derivative with stress protein-inducing activity and cytoprotective effects. *Nat. Med.* **3**, 1150–1154 (1997).
8. S. M. Gehrig, C. van der Poel, T. A. Sayer, J. D. Schertzer, D. C. Henstridge, J. E. Church, S. Lamon, A. P. Russell, K. E. Davies, M. A. Febbraio, G. S. Lynch, Hsp72 preserves muscle function and slows progression of severe muscular dystrophy. *Nature* **484**, 394–398 (2012).
9. J. Nylandsted, M. Gyrd-Hansen, A. Danielewicz, N. Fehrenbacher, U. Lademann, M. Høyer-Hansen, E. Weber, G. Multhoff, M. Rohde, M. Jäättelä, Heat shock protein 70 promotes cell survival by inhibiting lysosomal membrane permeabilization. *J. Exp. Med.* **200**, 425–435 (2004).
10. J.-H. Hwang, J. K. Ryu, Y. B. Yoon, K. H. Lee, Y.-S. Park, J.-W. Kim, N. Kim, D. H. Lee, J. B. Jeong, J.-S. Seo, Y.-T. Kim, Spontaneous activation of pancreas trypsinogen in heat shock protein 70.1 knock-out mice. *Pancreas* **31**, 332–336 (2005).
11. T. Kirkegaard, M. Jäättelä, Lysosomal involvement in cell death and cancer. *Biochim. Biophys. Acta* **1793**, 746–754 (2009).
12. T. Kolter, K. Sandhoff, Principles of lysosomal membrane digestion: Stimulation of sphingolipid degradation by sphingolipid activator proteins and anionic lysosomal lipids. *Annu. Rev. Cell Dev. Biol.* **21**, 81–103 (2005).
13. A. K. Mahalka, T. Kirkegaard, L. T. I. Jukola, M. Jäättelä, P. K. J. Kinnunen, Human heat shock protein 70 (Hsp70) as a peripheral membrane protein. *Biochim. Biophys. Acta* **1838**, 1344–1361 (2014).
14. S. Locatelli-Hoops, N. Remmel, R. Klingenstein, B. Breiden, M. Rossocha, M. Schoeniger, C. Koenigs, W. Saenger, K. Sandhoff, Saposin A mobilizes lipids from low cholesterol and high bis(monoacylglycerol)phosphate-containing membranes: Patient variant Saposin A lacks lipid extraction capacity. *J. Biol. Chem.* **281**, 32451–32460 (2006).
15. G. Wilkening, T. Linke, K. Sandhoff, Lysosomal degradation on vesicular membrane surfaces. Enhanced glucosylceramide degradation by lysosomal anionic lipids and activators. *J. Biol. Chem.* **273**, 30271–30278 (1998).
16. G. Wilkening, T. Linke, G. Uhlhorn-Dierks, K. Sandhoff, Degradation of membrane-bound ganglioside GM1. Stimulation by bis(monoacylglycero)phosphate and the activator proteins SAP-B and GM2-AP. *J. Biol. Chem.* **275**, 35814–35819 (2000).
17. T. Linke, G. Wilkening, F. Sadeghlar, H. Mozcall, K. Bernardo, E. Schuchman, K. Sandhoff, Interfacial regulation of acid ceramidase activity. Stimulation of ceramide degradation by lysosomal lipids and sphingolipid activator proteins. *J. Biol. Chem.* **276**, 5760–5768 (2001).
18. T. Linke, G. Wilkening, S. Lansmann, H. Moczall, O. Bartelsen, J. Weisgerber, K. Sandhoff, Stimulation of acid sphingomyelinase activity by lysosomal lipids and sphingolipid activator proteins. *Biol. Chem.* **382**, 283–290 (2001).
19. N. H. T. Petersen, T. Kirkegaard, HSP70 and lysosomal storage disorders: Novel therapeutic opportunities. *Biochem. Soc. Trans.* **38**, 1479–1483 (2010).
20. M. E. Guicciardi, M. Leist, G. J. Gores, Lysosomes in cell death. *Oncogene* **23**, 2881–2890 (2004).
21. M. C. Micsenyi, J. Sikora, G. Stephney, K. Dobrenis, S. U. Walkley, Lysosomal membrane permeability stimulates protein aggregate formation in neurons of a lysosomal disease. *J. Neurosci.* **33**, 10815–10827 (2013).
22. D. te Vruchte, A. O. Speak, K. L. Wallom, N. Al Eisa, D. A. Smith, C. J. Hendriksz, L. Simmons, R. H. Lachmann, A. Cousins, R. Hartung, E. Mengel, H. Runz, M. Beck, Y. Amraoui, J. Imrie, E. Jacklin, K. Riddick, N. M. Yanjanin, C. A. Wassif, A. Rolfs, F. Rimmele, N. Wright, C. Taylor, U. Ramaswami, T. M. Cox, C. Hastings, X. Jiang, R. Sidhu, D. S. Ory, B. Arias, M. Jeyakumar, D. J. Sillence, J. E. Wraith, F. D. Porter, M. Cortina-Borja, F. M. Platt, Relative acidic compartment volume as a lysosomal storage disorder-associated biomarker. *J. Clin. Invest.* **124**, 1320–1328 (2014).
23. N. H. T. Petersen, O. D. Olsen, L. Groth-Pedersen, A.-M. Ellegaard, M. Bilgin, S. Redmer, M. S. Ostenfeld, D. Ulanet, T. H. Dovmark, A. Lønborg, S. D. Vindeløv, D. Hanahan, C. Arenz, C. S. Ejsing, T. Kirkegaard, M. Rohde, J. Nylandsted, M. Jäättelä, Transformation-associated changes in sphingolipid metabolism sensitize cells to lysosomal cell death induced by inhibitors of acid sphingomyelinase. *Cancer Cell* **24**, 379–393 (2013).
24. R. A. Nixon, The role of autophagy in neurodegenerative disease. *Nat. Med.* **19**, 983–997 (2013).
25. M. S. Ostenfeld, M. Høyer-Hansen, L. Bastholm, N. Fehrenbacher, O. D. Olsen, L. Groth-Pedersen, P. Puustinen, T. Kirkegaard-Sorensen, J. Nylandsted, T. Farkas, M. Jäättelä, Anti-cancer agent siramesine is a lysosomotropic detergent that induces cytoprotective autophagosome accumulation. *Autophagy* **4**, 487–499 (2008).

26. N. W. Werneburg, M. E. Guicciardi, S. F. Bronk, G. J. Gores, Tumor necrosis factor-α-associated lysosomal permeabilization is cathepsin B dependent. *Am. J. Physiol. Gastrointest. Liver Physiol.* **283**, G947–G956 (2002).
27. T.-W. Mu, D. S. T. Ong, Y.-J. Wang, W. E. Balch, J. R. Yates III, L. Segatori, J. W. Kelly, Chemical and biological approaches synergize to ameliorate protein-folding diseases. *Cell* **134**, 769–781 (2008).
28. H. Zhu, T. Yoshimoto, T. Yamashima, Heat shock protein 70.1 (Hsp70.1) affects neuronal cell fate by regulating lysosomal acid sphingomyelinase. *J. Biol. Chem.* **289**, 27432–27443 (2014).
29. N. Nakasone, Y. S. Nakamura, K. Higaki, N. Oumi, K. Ohno, H. Ninomiya, Endoplasmic reticulum-associated degradation of Niemann-Pick C1: Evidence for the role of heat shock proteins and identification of lysine residues that accept ubiquitin. *J. Biol. Chem.* **289**, 19714–19725 (2014).
30. C. Yang, C. L. Swallows, C. Zhang, J. Lu, H. Xiao, R. O. Brady, Z. Zhuang, Celastrol increases glucocerebrosidase activity in Gaucher disease by modulating molecular chaperones. *Proc. Natl. Acad. Sci. U.S.A.* **111**, 249–254 (2014).
31. E. M. O'Leary, S. A. Igdoura, The therapeutic potential of pharmacological chaperones and proteosomal inhibitors, Celastrol and MG132 in the treatment of sialidosis. *Mol. Genet. Metab.* **107**, 173–185 (2012).
32. S. Zampieri, B. Bembi, N. Rosso, M. Filocamo, A. Dardis, Treatment of human fibroblasts carrying NPC1 missense mutations with MG132 leads to an improvement of intracellular cholesterol trafficking. *JIMD Rep.* **2**, 59–69 (2012).
33. L. Ingemann, T. Kirkegaard, Lysosomal storage diseases and the heat shock response: Convergences and therapeutic opportunities. *J. Lipid Res.* **55**, 2198–2210 (2014).
34. M. E. Cudkowicz, J. M. Shefner, E. Simpson, D. Grasso, H. Yu, H. Zhang, A. Shui, D. Schoenfeld, R. H. Brown, S. Wieland, J. R. Barber, Arimoclomol at dosages up to 300 mg/day is well tolerated and safe in amyotrophic lateral sclerosis. *Muscle Nerve* **38**, 837–844 (2008).
35. V. Lanka, S. Wieland, J. Barber, M. Cudkowicz, Arimoclomol: A potential therapy under development for ALS. *Expert Opin. Investig. Drugs* **18**, 1907–1918 (2009).
36. J. Anckar, L. Sistonen, Regulation of HSF1 function in the heat stress response: Implications in aging and disease. *Annu. Rev. Biochem.* **80**, 1089–1115 (2011).
37. T. Crul, N. Toth, S. Piotto, P. Literati-Nagy, K. Tory, P. Haldimann, B. Kalmar, L. Greensmith, Z. Torok, G. Balogh, I. Gombos, F. Campana, S. Concilio, F. Gallyas, G. Nagy, Z. Berente, B. Gungor, M. Peter, A. Glatz, A. Hunya, Z. Literati-Nagy, L. Vigh, F. Hoogstra-Berends, A. Heeres, I. Kuipers, L. Loen, J.-P. Seerden, D. Zhang, R. A. M. Meijering, R. H. Henning, B. J. J. M. Brundel, H. H. Kampinga, L. Koranyi, Z. Szilvassy, J. Mandl, B. Sumegi, M. A. Febbraio, I. Horvath, P. L. Hooper, L. Vigh, Hydroximic acid derivatives: Pleiotropic HSP co-inducers restoring homeostasis and robustness. *Curr. Pharm. Des.* **19**, 309–346 (2013).
38. D. A. Parfitt, M. Aguila, C. H. McCulley, D. Bevilacqua, H. F. Mendes, D. Athanasiou, S. S. Novoselov, N. Kanuga, P. M. Munro, P. J. Coffey, B. Kalmar, L. Greensmith, M. E. Cheetham, The heat-shock response co-inducer arimoclomol protects against retinal degeneration in rhodopsin retinitis pigmentosa. *Cell Death Dis.* **5**, e1236 (2014).
39. E. Lloyd-Evans, A. J. Morgan, X. He, D. A. Smith, E. Elliot-Smith, D. J. Sillence, G. C. Churchill, E. H. Schuchman, A. Galione, F. M. Platt, Niemann-Pick disease type C1 is a sphingosine storage disease that causes deregulation of lysosomal calcium. *Nat. Med.* **14**, 1247–1255 (2008).
40. C. Devlin, N. H. Pipalia, X. Liao, E. H. Schuchman, F. R. Maxfield, I. Tabas, Improvement in lipid and protein trafficking in Niemann-Pick C1 cells by correction of a secondary enzyme defect. *Traffic* **11**, 601–615 (2010).
41. J. Chevallier, Z. Chamoun, G. Jiang, G. Prestwich, N. Sakai, S. Matile, R. G. Parton, J. Gruenberg, Lysobisphosphatidic acid controls endosomal cholesterol levels. *J. Biol. Chem.* **283**, 27871–27880 (2008).
42. Y. Sugimoto, H. Ninomiya, Y. Ohsaki, K. Higaki, J. P. Davies, Y. A. Ioannou, K. Ohno, Accumulation of cholera toxin and GM1 ganglioside in the early endosome of Niemann–Pick C1-deficient cells. *Proc. Natl. Acad. Sci. U.S.A.* **98**, 12391–12396 (2001).
43. M. Daugaard, M. Rohde, M. Jäättelä, The heat shock protein 70 family: Highly homologous proteins with overlapping and distinct functions. *FEBS Lett.* **581**, 3702–3710 (2007).
44. E. A. A. Nollen, R. I. Morimoto, Chaperoning signaling pathways: Molecular chaperones as stress-sensing 'heat shock' proteins. *J. Cell Sci.* **115**, 2809–2816 (2002).
45. E. C. M. de Lange, P. G. M. Ravenstijn, D. Groenendaal, T. J. van Steeg, Toward the prediction of CNS drug-effect profiles in physiological and pathological conditions using microdialysis and mechanism-based pharmacokinetic-pharmacodynamic modeling. *AAPS J.* **7**, E532–E543 (2005).
46. D. Triguero, J. Buciak, W. M. Pardridge, Capillary depletion method for quantification of blood–brain barrier transport of circulating peptides and plasma proteins. *J. Neurochem.* **54**, 1882–1888 (1990).
47. C. S. Patlak, R. G. Blasberg, J. D. Fenstermacher, Graphical evaluation of blood-to-brain transfer constants from multiple-time uptake data. *J. Cereb. Blood Flow Metab.* **3**, 1–7 (1983).
48. R. Gabathuler, Approaches to transport therapeutic drugs across the blood–brain barrier to treat brain diseases. *Neurobiol. Dis.* **37**, 48–57 (2010).
49. S. Takemoto, M. Nishikawa, Y. Takakura, Pharmacokinetic and tissue distribution mechanism of mouse recombinant heat shock protein 70 in mice. *Pharm. Res.* **22**, 419–426 (2005).
50. S. Basu, R. J. Binder, T. Ramalingam, P. K. Srivastava, CD91 is a common receptor for heat shock proteins gp96, hsp90, hsp70, and calreticulin. *Immunity* **14**, 303–313 (2001).
51. T. Becker, F.-U. Hartl, F. Wieland, CD40, an extracellular receptor for binding and uptake of Hsp70–peptide complexes. *J. Cell Biol.* **158**, 1277–1285 (2002).
52. C. Gross, D. Hansch, R. Gastpar, G. Multhoff, Interaction of heat shock protein 70 peptide with NK cells involves the NK receptor CD94. *Biol. Chem.* **384**, 267–279 (2003).
53. M. Demeule, J.-C. Currie, Y. Bertrand, C. Ché, T. Nguyen, A. Régina, R. Gabathuler, J.-P. Castaigne, R. Béliveau, Involvement of the low-density lipoprotein receptor-related protein in the transcytosis of the brain delivery vector angiopep-2. *J. Neurochem.* **106**, 1534–1544 (2008).
54. T. Kirkegaard, Emerging therapies and therapeutic concepts for lysosomal storage diseases. *Expert Opin. Orphan Drugs* **1**, 385–404 (2013).
55. P. G. Pentchev, A. D. Boothe, H. S. Kruth, H. Weintroub, J. Stivers, R. O. Brady, A genetic storage disorder in BALB/C mice with a metabolic block in esterification of exogenous cholesterol. *J. Biol. Chem.* **259**, 5784–5791 (1984).
56. T. Ohshima, G. J. Murray, W. D. Swaim, G. Longenecker, J. M. Quirk, C. O. Cardarelli, Y. Sugimoto, I. Pastan, M. M. Gottesman, R. O. Brady, A. B. Kulkarni, α-Galactosidase A deficient mice: A model of Fabry disease. *Proc. Natl. Acad. Sci. U.S.A.* **94**, 2540–2544 (1997).
57. K. Sango, S. Yamanaka, A. Hoffmann, Y. Okuda, A. Grinberg, H. Westphal, M. P. McDonald, J. N. Crawley, K. Sandhoff, K. Suzuki, R. L. Proia, Mouse models of Tay–Sachs and Sandhoff diseases differ in neurologic phenotype and ganglioside metabolism. *Nat. Genet.* **11**, 170–176 (1995).
58. D. Phaneuf, N. Wakamatsu, J.-Q. Huang, A. Borowski, A. C. Peterson, S. R. Fortunato, G. Ritter, S. A. Igdoura, C. R. Morales, G. Benoit, B. R. Akerman, D. Leclerc, N. Hanai, J. D. Marth, J. M. Trasler, R. A. Gravel, Dramatically different phenotypes in mouse models of human Tay-Sachs and Sandhoff diseases. *Hum. Mol. Genet.* **5**, 1–14 (1996).
59. Y. A. Ioannou, K. M. Zeidner, R. E. Gordon, R. J. Desnick, Fabry disease: Preclinical studies demonstrate the effectiveness of α-galactosidase A replacement in enzyme-deficient mice. *Am. J. Hum. Genet.* **68**, 14–25 (2001).
60. J. M. F. G. Aerts, W. W. Kallemeijn, W. Wegdam, M. Joao Ferraz, M. J. van Breemen, N. Dekker, G. Kramer, B. J. Poorthuis, J. E. M. Groener, J. Cox-Brinkman, S. M. Rombach, C. E. M. Hollak, G. E. Linthorst, M. D. Witte, H. Gold, G. A. van der Marel, H. S. Overkleeft, R. G. Boot, Biomarkers in the diagnosis of lysosomal storage disorders: Proteins, lipids, and inhibodies. *J. Inherit. Metab. Dis.* **34**, 605–619 (2011).
61. A. Abe, S. Gregory, L. Lee, P. D. Killen, R. O. Brady, A. Kulkarni, J. A. Shayman, Reduction of globotriaosylceramide in Fabry disease mice by substrate deprivation. *J. Clin. Invest.* **105**, 1563–1571 (2000).
62. A. O. Speak, M. Salio, D. C. A. Neville, J. Fontaine, D. A. Priestman, N. Platt, T. Heare, T. D. Butters, R. A. Dwek, F. Trottein, M. A. Exley, V. Cerundolo, F. M. Platt, Implications for invariant natural killer T cell ligands due to the restricted presence of isoglobotrihexosylceramide in mammals. *Proc. Natl. Acad. Sci. U.S.A.* **104**, 5971–5976 (2007).
63. M. Jeyakumar, T. D. Butters, M. Cortina-Borja, V. Hunnam, R. L. Proia, V. H. Perry, R. A. Dwek, F. M. Platt, Delayed symptom onset and increased life expectancy in Sandhoff disease mice treated with *N*-butyldeoxynojirimycin. *Proc. Natl. Acad. Sci. U.S.A.* **96**, 6388–6393 (1999).
64. M. Zervas, K. L. Somers, M. A. Thrall, S. U. Walkley, Critical role for glycosphingolipids in Niemann-Pick disease type C. *Curr. Biol.* **11**, 1283–1287 (2001).
65. M. T. Vanier, Niemann-Pick disease type C. *Orphanet J. Rare Dis.* **5**, 16 (2010).
66. S. U. Walkley, M. T. Vanier, Secondary lipid accumulation in lysosomal disease. *Biochim. Biophys. Acta* **1793**, 726–736 (2009).
67. G. Vaquer, F. Rivière Dannerstedt, M. Mavris, F. Bignami, J. Llinares-Garcia, K. Westermark, B. Sepodes, Animal models for metabolic, neuromuscular and ophthalmological rare diseases. *Nat. Rev. Drug Discov.* **12**, 287–305 (2013).
68. M. Walterfang, M. Fahey, P. Desmond, A. Wood, M. L. Seal, C. Steward, C. Adamson, C. Kokkinos, M. Fietz, D. Velakoulis, White and gray matter alterations in adults with Niemann-Pick disease type C: A cross-sectional study. *Neurology* **75**, 49–56 (2010).
69. T. Yu, A. P. Lieberman, Npc1 acting in neurons and glia is essential for the formation and maintenance of CNS myelin. *PLOS Genet.* **9**, e1003462 (2013).
70. M. T. Vanier, Lipid changes in Niemann-Pick disease type C brain: Personal experience and review of the literature. *Neurochem. Res.* **24**, 481–489 (1999).
71. S. Takikita, T. Fukuda, I. Mohri, T. Yagi, K. Suzuki, Perturbed myelination process of premyelinating oligodendrocyte in Niemann-Pick type C mouse. *J. Neuropathol. Exp. Neurol.* **63**, 660–673 (2004).
72. M. Walterfang, M. D. Macfarlane, J. C. L. Looi, L. Abel, E. Bowman, M. C. Fahey, P. Desmond, D. Velakoulis, Pontine-to-midbrain ratio indexes ocular-motor function and illness stage in adult Niemann–Pick disease type C. *Eur. J. Neurol.* **19**, 462–467 (2012).
73. M. Walterfang, M. Fahey, L. Abel, M. Fietz, A. Wood, E. Bowman, D. Reutens, D. Velakoulis, Size and shape of the corpus callosum in adult Niemann-Pick type C reflects state and trait illness variables. *AJNR Am. J. Neuroradiol.* **32**, 1340–1346 (2011).
74. X. Yan, J. Lukas, M. Witt, A. Wree, R. Hübner, M. Frech, R. Köhling, A. Rolfs, J. Luo, Decreased expression of myelin gene regulatory factor in Niemann-Pick type C 1 mouse. *Metab. Brain Dis.* **26**, 299–306 (2011).
75. R. L. Schnaar, Brain gangliosides in axon-myelin stability and axon regeneration. *FEBS Lett.* **584**, 1741–1747 (2010).
76. R. K. Yu, Y. Nakatani, M. Yanagisawa, The role of glycosphingolipid metabolism in the developing brain. *J. Lipid Res.* **50**, S440–S445 (2009).

77. A. Tessitore, M. del P. Martin, R. Sano, Y. Ma, L. Mann, A. Ingrassia, E. D. Laywell, D. A. Steindler, L. M. Hendershot, A. d'Azzo, GM1-ganglioside-mediated activation of the unfolded protein response causes neuronal death in a neurodegenerative gangliosidosis. *Mol. Cell* **15**, 753–766 (2004).
78. R. Sano, I. Annunziata, A. Patterson, S. Moshiach, E. Gomero, J. Opferman, M. Forte, A. d'Azzo, GM1-ganglioside accumulation at the mitochondria-associated ER membranes links ER stress to Ca^{2+}-dependent mitochondrial apoptosis. *Mol. Cell* **36**, 500–511 (2009).
79. B. Kalmar, C.-H. Lu, L. Greensmith, The role of heat shock proteins in amyotrophic lateral sclerosis: The therapeutic potential of arimoclomol. *Pharmacol. Ther.* **141**, 40–54 (2014).
80. M. Benatar, J. Kurent, D. H. Moore, Treatment for familial amyotrophic lateral sclerosis/motor neuron disease. *Cochrane Database Syst. Rev.* CD006153 (2009).
81. J. Macías-Vidal, M. Girós, M. Guerrero, P. Gascón, J. Serratosa, O. Bachs, M. J. Coll, The proteasome inhibitor bortezomib reduced cholesterol accumulation in fibroblasts from Niemann-Pick type C patients carrying missense mutations. *FEBS J.* **281**, 4450–4466 (2014).
82. R. I. Morimoto, The heat shock response: Systems biology of proteotoxic stress in aging and disease. *Cold Spring Harb. Symp. Quant. Biol.* **76**, 91–99 (2011).
83. B. Malik, N. Nirmalananthan, A. L. Gray, A. R. La Spada, M. G. Hanna, L. Greensmith, Co-induction of the heat shock response ameliorates disease progression in a mouse model of human spinal and bulbar muscular atrophy: Implications for therapy. *Brain* **136** (Pt. 3), 926–943 (2013).
84. C. Yang, S. Rahimpour, J. Lu, K. Pacak, B. Ikejiri, R. O. Brady, Z. Zhuang, Histone deacetylase inhibitors increase glucocerebrosidase activity in Gaucher disease by modulation of molecular chaperones. *Proc. Natl. Acad. Sci. U.S.A.* **110**, 966–971 (2013).
85. R. I. Morimoto, Proteotoxic stress and inducible chaperone networks in neurodegenerative disease and aging. *Genes Dev.* **22**, 1427–1438 (2008).
86. M. Jäättelä, Heat shock proteins as cellular lifeguards. *Ann. Med.* **31**, 261–271 (1999).
87. C. D. Davidson, N. F. Ali, M. C. Micsenyi, G. Stephney, S. Renault, K. Dobrenis, D. S. Ory, M. T. Vanier, S. U. Walkley, Chronic cyclodextrin treatment of murine Niemann-Pick C disease ameliorates neuronal cholesterol and glycosphingolipid storage and disease progression. *PLOS One* **4**, e6951 (2009).
88. V. M. Stein, A. Crooks, W. Ding, M. Prociuk, P. O'Donnell, C. Bryan, T. Sikora, J. Dingemanse, M. T. Vanier, S. U. Walkley, C. H. Vite, Miglustat improves Purkinje cell survival and alters microglial phenotype in feline Niemann-Pick disease type C. *J. Neuropathol. Exp. Neurol.* **71**, 434–448 (2012).
89. J. B. Nietupski, J. J. Pacheco, W.-L. Chuang, K. Maratea, L. Li, J. Foley, K. M. Ashe, C. G. F. Cooper, J. M. F. G. Aerts, D. P. Copeland, R. K. Scheule, S. H. Cheng, J. Marshall, Iminosugar-based inhibitors of glucosylceramide synthase prolong survival but paradoxically increase brain glucosylceramide levels in Niemann-Pick C mice. *Mol. Genet. Metab.* **105**, 621–628 (2012).
90. N. H. Pipalia, C. C. Cosner, A. Huang, A. Chatterjee, P. Bourbon, N. Farley, P. Helquist, O. Wiest, F. R. Maxfield, Histone deacetylase inhibitor treatment dramatically reduces cholesterol accumulation in Niemann-Pick type C1 mutant human fibroblasts. *Proc. Natl. Acad. Sci. U.S.A.* **108**, 5620–5625 (2011).
91. K. J. Dean, C. C. Sweeley, Studies on human liver α-galactosidases. II. Purification and enzymatic properties of α-galactosidase B (α-*N*-acetylgalactosaminidase). *J. Biol. Chem.* **254**, 10001–10005 (1979).
92. M. E. Gelsthorpe, N. Baumann, E. Millard, S. E. Gale, S. J. Langmade, J. E. Schaffer, D. S. Ory, Niemann-Pick type C1 I1061T mutant encodes a functional protein that is selected for endoplasmic reticulum-associated degradation due to protein misfolding. *J. Biol. Chem.* **283**, 8229–8236 (2008).
93. E. Mengel, H.-H. Klünemann, C. M. Lourenço, C. J. Hendriksz, F. Sedel, M. Walterfang, S. A. Kolb, Niemann-Pick disease type C symptomatology: An expert-based clinical description. *Orphanet J. Rare Dis.* **8**, 166 (2013).
94. M. Praggastis, B. Tortelli, J. Zhang, H. Fujiwara, R. Sidhu, A. Chacko, Z. Chen, C. Chung, A. P. Lieberman, J. Sikora, C. Davidson, S. U. Walkley, N. H. Pipalia, F. R. Maxfield, J. E. Schaffer, D. S. Ory, A murine Niemann-Pick C1 I1061T knock-in model recapitulates the pathological features of the most prevalent human disease allele. *J. Neurosci.* **35**, 8091–8106 (2015).
95. D. J. Gifondorwa, M. B. Robinson, C. D. Hayes, A. R. Taylor, D. M. Prevette, R. W. Oppenheim, J. Caress, C. E. Milligan, Exogenous delivery of heat shock protein 70 increases lifespan in a mouse model of amyotrophic lateral sclerosis. *J. Neurosci.* **27**, 13173–13180 (2007).
96. J. C. Plumier, B. M. Ross, R. W. Currie, C. E. Angelidis, H. Kazlaris, G. Kollias, G. N. Pagoulatos, Transgenic mice expressing the human heat shock protein 70 have improved post-ischemic myocardial recovery. *J. Clin. Invest.* **95**, 1854–1860 (1995).
97. M. S. Marber, R. Mestril, S. H. Chi, M. R. Sayen, D. M. Yellon, W. H. Dillmann, Overexpression of the rat inducible 70-kD heat stress protein in a transgenic mouse increases the resistance of the heart to ischemic injury. *J. Clin. Invest.* **95**, 1446–1456 (1995).
98. M. Ahmed, P. M. Machado, A. Miller, C. Spicer, L. Herbelin, J. He, J. Noel, Y. Wang, A. L. McVey, M. Pasnoor, P. Gallagher, J. Statland, C.-H. Lu, B. Kalmar, S. Brady, H. Sethi, G. Samandouras, M. Parton, J. L. Holton, A. Weston, L. Collinson, J. P. Taylor, G. Schiavo, M. G. Hanna, R. J. Barohn, M. M. Dimachkie, L. Greensmith, Targeting protein homeostasis in sporadic inclusion body myositis. *Sci. Transl. Med.* **8**, 331ra41 (2016).
99. E. Lloyd-Evans, F. M. Platt, Lipids on trial: The search for the offending metabolite in Niemann-Pick type C disease. *Traffic* **11**, 419–428 (2010).
100. F. M. Platt, Sphingolipid lysosomal storage disorders. *Nature* **510**, 68–75 (2014).
101. A. Buchberger, B. Bukau, T. Sommer, Protein quality control in the cytosol and the endoplasmic reticulum: Brothers in arms. *Mol. Cell* **40**, 238–252 (2010).
102. B. Kalmar, G. Burnstock, G. Vrbová, R. Urbanics, P. Csermely, L. Greensmith, Upregulation of heat shock proteins rescues motoneurones from axotomy-induced cell death in neonatal rats. *Exp. Neurol.* **176**, 87–97 (2002).
103. M. Kürthy, T. Mogyorósi, K. Nagy, T. Kukorelli, A. Jednákovits, L. Tálosi, K. Bíró, Effect of BRX-220 against peripheral neuropathy and insulin resistance in diabetic rat models. *Ann. N. Y. Acad. Sci.* **967**, 482–489 (2002).
104. B. Kalmar, S. Novoselov, A. Gray, M. E. Cheetham, B. Margulis, L. Greensmith, Late stage treatment with arimoclomol delays disease progression and prevents protein aggregation in the $SOD1^{G93A}$ mouse model of ALS. *J. Neurochem.* **107**, 339–350 (2008).
105. T. I. F. H. Cremers, G. Flik, C. Hofland, R. E. Stratford Jr., Microdialysis evaluation of clozapine and *N*-desmethylclozapine pharmacokinetics in rat brain. *Drug Metab. Dispos.* **40**, 1909–1916 (2012).
106. D. J. Begley, D. G. Chain, Proceedings of the Physiological Society, 24–25 February 1984, Imperial College Meeting: Demonstrations. *J. Physiol.* **351**, 1–8 (1984).
107. S. K. Loftus, J. A. Morris, E. D. Carstea, J. Z. Gu, C. Cummings, A. Brown, J. Ellison, K. Ohno, M. A. Rosenfeld, D. A. Tagle, P. G. Pentchev, W. J. Pavan, Murine model of Niemann-Pick C disease: Mutation in a cholesterol homeostasis gene. *Science* **277**, 232–235 (1997).
108. D. C. A. Neville, V. Coquard, D. A. Priestman, D. J. M. te Vruchte, D. J. Sillence, R. A. Dwek, F. M. Platt, T. D. Butters, Analysis of fluorescently labeled glycosphingolipid-derived oligosaccharides following ceramide glycanase digestion and anthranilic acid labeling. *Anal. Biochem.* **331**, 275–282 (2004).
109. J. Folch, M. Lees, G. H. Sloane Stanley, A simple method for the isolation and purification of total lipides from animal tissues. *J. Biol. Chem.* **226**, 497–509 (1957).
110. E. Elliot-Smith, A. O. Speak, E. Lloyd-Evans, D. A. Smith, A. C. van der Spoel, M. Jeyakumar, T. D. Butters, R. A. Dwek, A. d'Azzo, F. M. Platt, Beneficial effects of substrate reduction therapy in a mouse model of GM1 gangliosidosis. *Mol. Genet. Metab.* **94**, 204–211 (2008).

Acknowledgments: We thank E. Schuchman for NPDA (B534) cells, and K. Sandhoff and H. Schulze for NPDA 83/24 and Farber 89/78 and 89/73 cells. **Funding:** T.K. received a pre-seed grant from the Novo Nordisk Foundation. F.M.P. is a Royal Society Wolfson Research Merit Award holder. J.G., I.W., K.-L.W., and D.A.P. were supported by grants from Orphazyme. This project was supported by grants from the Danish Cancer Society (R90-A5783), the Danish Medical Research Council (10-083790), the European Research Council (AdG 340751), and the Danish National Research Foundation (DNRF125) for M.J. C.A. and A.K. are grateful for financial support by the Deutsche Forschungsgemeinschaft. J.G. was supported by Wellcome Trust Pathfinder grant 105687/Z/14/Z. **Author contributions:** T.K. conceived and designed the studies for Figs. 1, 2, and 6 (A and B) and figs. S3 and S4; analyzed the data; and wrote and edited the paper. T.K., F.P., and J.G. conceived and designed the studies for Figs. 3 to 5 and 6 (C and D) and figs. S1 and S2 and analyzed the data. M.J. supervised and edited the paper. F.P. supervised, analyzed the data, and edited the paper. D.A.P. designed the studies for Fig. 3 and analyzed the data. K.-L.W. designed the studies for Fig. 4 and analyzed the data. D.B. and S.D. designed and analyzed the studies for Fig. 2H and Table 1. O.D.O. performed experiments and analyzed data for Figs. 1 (C and D) and 2 (C and D). N.H.T.P. performed experiments and analyzed data for Fig. 6 (C and D). L.I. performed experiments and analyzed data for Figs. 1B and 6A and fig. S4. S.H.J. designed the studies for Figs. 5F and 6 (B to F) and analyzed and discussed data. D.A.S. and L.M. aided in design, performance of experiments, and analysis of data for Figs. 3 to 6. C.B. designed and performed experiments and analyzed data for Fig. 6A and fig. S5. I.W. supervised J.G. and aided in experimental setup. A.H. analyzed data for fig. S1 and provided analytical support and discussions for all experiments. C.A. and A.K. designed and performed the experiments and analyzed the data for Fig. 1A. C.A. supervised A.K. All authors discussed the results and commented on the manuscript. **Competing interests:** T.K. and M.J. hold shares in Orphazyme. T.K. and M.J. are inventors on patents related to this work [PCT/DK2009/050151, "Use of Hsp70 protein or small molecule inducers of HSPs, including Hsp70, for the treatment of lysosomal storage disorders (LSD)"; PCT/DK2011/050444, "Use of Hsp70 protein or small molecule HSP inducers for the treatment of additional lysosomal storage disorders (LSD)"]. D.B. is a consultant for Alexion and Cyclodextrin Technology Development Holdings. F.P. is a consultant for Orphazyme and Actelion.

Submitted 2 December 2015
Accepted 18 August 2016
Published 7 September 2016
10.1126/scitranslmed.aad9823

Citation: T. Kirkegaard, J. Gray, D. A. Priestman, K.-L. Wallom, J. Atkins, O. D. Olsen, A. Klein, S. Drndarski, N. H. T. Petersen, L. Ingemann, D. A. Smith, L. Morris, C. Bornæs, S. H. Jørgensen, I. Williams, A. Hinsby, C. Arenz, D. Begley, M. Jäättelä, F. M. Platt, Heat shock protein–based therapy as a potential candidate for treating the sphingolipidoses. *Sci. Transl. Med.* **8**, 355ra118 (2016).

Science Translational Medicine
AAAS

Heat shock protein–based therapy as a potential candidate for treating the sphingolipidoses

Thomas Kirkegaard, James Gray, David A. Priestman, Kerri-Lee Wallom, Jennifer Atkins, Ole Dines Olsen, Alexander Klein, Svetlana Drndarski, Nikolaj H. T. Petersen, Linda Ingemann, David A. Smith, Lauren Morris, Claus Bornæs, Signe Humle Jørgensen, Ian Williams, Anders Hinsby, Christoph Arenz, David Begley, Marja Jäättelä and Frances M. Platt (September 7, 2016)
Science Translational Medicine **8** (355), 355ra118. [doi: 10.1126/scitranslmed.aad9823]

Editor's Summary

Heat shock protein to the rescue

The sphingolipidoses constitute a major subgroup of lysosomal storage diseases, a class of inherited metabolic disorders characterized by severe systemic and neurological problems. Few therapeutic options exist for treating these disorders. Kirkegaard *et al*. now demonstrate that increasing the expression of the molecular chaperone HSP70 through administration of either recombinant human HSP70 or the clinically tested, orally available small-molecule arimoclomol ameliorated disease manifestations, including brain pathology, in several different animal models of sphingolipidoses.

Science Translational Medicine (print ISSN 1946-6234; online ISSN 1946-6242) is published weekly, except the last week in December, by the American Association for the Advancement of Science, 1200 New York Avenue, NW, Washington, DC 20005.